Journal of Molecular Spectroscopy 267 (2011) 23–35

Contents lists available at ScienceDirect

Journal of Molecular Spectroscopy

journal homepage: www.elsevier.com/locate/jms

Approximate theoretical model for the five electronic states (Ω = 5/2, 3/2, 3/2, 1/2, 1/2) arising from the ground $3d^9$ configuration in nickel halide molecules and for rotational levels of the two Ω = 1/2 states in that manifold

Jon T. Hougen *

Optical Technology Division, National Institute of Standards and Technology, Gaithersburg, MD 20899-8441, USA

ARTICLE INFO

Article history:
Available online 25 January 2011

Keywords:
Electronic states
d-Electrons
Crystal-field theory
Spin–orbit components
Rotational levels
p-Type doubling
Ω = 1/2 states

ABSTRACT

In the first part of this paper an effective Hamiltonian for a non-rotating diatomic molecule containing only crystal-field and spin–orbit operators is set up to describe the energies of the five spin–orbit components that arise in the ground electronic configuration of the nickel monohalides. The model assumes that bonding in the nickel halides has the approximate form Ni^+X^-, with an electronic $3d^9$ configuration plus closed shells on the Ni^+ moiety and a closed shell configuration on the X^- moiety. From a crystal-field point of view, interactions of the positive *d*-hole with the cylindrically symmetrical electric charge distribution of the hypothetical NiX^- closed-shell core can then be parameterized by three terms in a traditional expansion in spherical harmonics: $C_0 + C_2Y_{20}(\theta, \phi) + C_4Y_{40}(\theta, \phi)$. Interaction of the hole with the magnetic field generated by its own orbital motion can be parameterized by a traditional spin–orbit interaction operator $A\boldsymbol{L}\cdot\boldsymbol{S}$. The Hamiltonian matrix is set up in a basis set consisting of the 10 Hund's case (a) basis functions $|L, \Lambda; S, \Sigma\rangle$ that arise when $L = 2$ and $S = 1/2$. Least-squares fits of the observed five spin–orbit components of the three lowest electronic states in NiF and NiCl are then carried out in terms of the four parameters C_0, C_2, C_4, and A which lead to good agreement, except for the two $|\Omega| = 1/2$ states. The large equal and opposite residuals of the $|\Omega| = 1/2$ states can be reduced to values comparable with those for the $|\Omega| = 3/2$ and $|\Omega| = 5/2$ states by fixing A to its value in Ni^+ and then introducing an empirical correction factor for one off-diagonal orbital matrix element. In the second part of this paper the usual effective Hamiltonian $B(\boldsymbol{J}-\boldsymbol{L}-\boldsymbol{S})^2$ for a rotating diatomic molecule is used to derive expressions for the Ω-type doubling parameter p in the two $|\Omega| = 1/2$ states. These expressions show (for certain sign conventions) that the sum of the two p values should be $-2B$, but that their difference can vary between $-10B$ and $+10B$. These theoretical results are in good agreement with the two observed p values for both NiF and NiCl. The present formalism should in principle be applicable to NiBr and NiI, and to the halides of palladium, since Pd^+ has a well isolated $4d^9$ electronic ground configuration. Extension to metal halides having d^n configurations with $n < 9$, or to platinum halides may present difficulties, since manifolds from the d^n and $d^{n-1}s$ configurations may be heavily mixed, thus requiring "too many" parameters in the electronic part of the problem. Application to linear triatomic molecules may also present problems because of the large number of vibronic perturbations made possible by their four vibrational degrees of freedom.

1. Introduction

A large number of papers have appeared over the last 20 years in which the electronic and microwave spectra of the four nickel monohalides (NiX) and of nickel monohydride (NiH) have been studied experimentally. Examples of such studies (with rotational resolution) are: NiF [1–7], NiCl [8–14], NiBr [15–17], NiI [18–21], and NiH [22–26]. The electronic states of these and related molecules have also been studied theoretically [27–32]. From the point of view of the present paper, we are interested in the following information extracted from these works.

The basic model consists of representing NiX as a singly charged Ni^+ ion bonded to a singly charged X^- ion. The isolated X^- atomic ion has a $^1S_0$ electronic ground state. Since excitations of these closed-shell electrons are ignored here, only the average charge distribution of the X^- ion is of interest. The isolated Ni^+ atomic ion has an $[Ar]3d^9$ ground electronic configuration [33], and the $L = 2$ and $S = 1/2$ angular momenta of its *d* hole give rise to atomic $^2D_{3/2}$ and $^2D_{5/2}$ states, which are split by 1506.94 cm^{-1} [33], leading to a free-ion spin–orbit constant $A = -602.8$ cm^{-1}.

When the two ions combine to form a molecule, we expect (from a simple one-configuration model) that the spin–orbit coupling constant of the molecule will remain close to the atomic value. A more noticeable effect of molecule formation, however, arises from the perturbation of the atomic *d*-orbital energy in the

* Fax: +1 301 975 2950.
E-mail address: jon.hougen@nist.gov

0022-2852/$ - see front matter © 2011 Elsevier Inc. All rights reserved.
doi:10.1016/j.jms.2011.01.007

Ni^+ ion by the electrostatic field of the X^- ion, which can be thought of as splitting the free-ion states into three Hund's case (b) [34] electronic states of symmetry $^2\Sigma^+$, $^2\Pi$, and $^2\Delta$, or into five Hund's case (c) states (i.e., five spin–orbit components of the three case (b) states) with $|\Omega| = 1/2$, 1/2, 3/2, 3/2, and 5/2. Such an electrostatic perturbation of atomic energy levels is often referred to as a crystal-field effect [35], because electrostatic models of various symmetries were used in many early studies of the colors of ionic crystals containing transition-metal or rare-earth cations. The crystal-field and spin–orbit forces compete with each other to determine the good quantum numbers, and thus also the energy level pattern, in the non-rotating molecule.

Coriolis forces generated when the molecule rotates then further attempt (via various $\Delta\Omega = \pm 1$ mixings) to dictate the choice of good quantum numbers in the final electronic-rotational wavefunctions, which leads in NiX and NiH to very large Ω-doubling splittings in the $\Omega = 1/2$ states (or equivalently, to very large spin-rotation splittings when the $\Omega = 1/2$ state is treated as a $^2\Sigma$ state). The various phenomena arising from such Coriolis mixings are often associated with the words *L*-uncoupling and *S*-uncoupling in discussions of Hund's coupling cases [34].

The goal of the present paper is to derive expressions relating the positions of the five spin–orbit components in the $3d^9$ manifold to the sign and magnitude of the Ω-doubling constant p in each of the two $\Omega = 1/2$ states in this manifold. Such expressions can then be used to check rotational assignments in the sometimes confusing $\Omega = 1/2$ states.

The quantum mechanical formalism used here is extremely similar to that presented two decades ago in a beautiful treatment of the electronic-rotational states of "the $\{Ni^+\ 3d^9\ ^2D\}$ supermultiplet" [27], and the reader is referred to that paper for much explanatory material not repeated here. The main differences in the present formalism are: (i) the use of three crystal-field parameters, rather than three term values, to describe the positions of the Hund's case (b) $^2\Sigma^+$, $^2\Pi$, and $^2\Delta$ electronic states arising from the Ni^+ ^2D atomic state, and (ii) the use of only 1×1 and 2×2 Hamiltonian matrices to calculate the nickel monohalide rotational levels. The change in viewpoint (i) was introduced in the hope that variation of empirical crystal-field parameters of NiX across the four halides (X = F, Cl, Br, I) will give additional chemical insight. The simplification (ii) was introduced because $B_{NiX} \ll B_{NiH}$, so that many of the *L*-uncoupling and *S*-uncoupling interactions that must be treated by exact diagonalization in NiH [27], can be treated by second-order perturbation theory in the nickel halides [16,17,21]. Note also that perturbations arising from $\Delta v \neq 0$ interactions among the $3d^9$ electronic states [27] are missing from these small matrices.

The treatment below should in principle be applicable without change to the halides of palladium, since Pd^+ has a well isolated $4d^9$ electronic ground configuration [33]. For Pt^+, however, some levels of $5d^9$ and $5d^86s$ are interleaved [33], which violates one of the assumptions of the model. The treatment below may also be applicable to the ground vibrational levels of $3d^9$ electronic states in linear triatomic molecules like NiCN [32,36], provided that complications due to the Renner–Teller effect and/or the larger number of vibrational modes can be ignored.

2. Theoretical model

As is often done in the diatomic literature, we divide our model into two parts, one dealing with the non-rotating molecule [27–32], the other dealing with the rotating molecule [27]. The reader is referred to Ref. [37] for a pedagogical description and algebraic details of this way of thinking as applied here. Symbolically, we can write

$$H = H_{non\text{-}rot} + H_{rot} = H_{cf} + H_{so} + H_{rot}, \tag{1}$$

where $H_{non\text{-}rot}$ is further divided, after the second equality, into a crystal-field (*cf*) term and a spin–orbit (*so*) term.

2.1. Non-rotating-molecule Hamiltonian operator and basis set

Since the electronic part of the present problem involves only one *d*-hole outside of closed shells, the only operator of interest in the separated ions is that describing spin–orbit interaction [38],

$$H_{so} = A\boldsymbol{L}\cdot\boldsymbol{S}, \tag{2}$$

which depends on the spin–orbit coupling constant A and on the orbital ($L = 2$) and spin ($S = 1/2$) angular momenta of the *d*-hole.

The electrostatic crystal-field perturbation of the *d*-orbital caused by the axial field of the diatomic molecule [28,29] can in principle be expressed as an infinite series in spherical harmonics $Y_{\ell m}(\theta, \varphi)$ centered on the Ni nucleus [35], where θ is the polar angle and φ is the azimuthal angle of the *d*-hole. This infinite series can be severely truncated for the present problem by noting that: (i) the electrostatic field has cylindrical symmetry, which requires $m = 0$ for all allowed terms in the series; (ii) we consider only matrix elements between states within the same electronic configuration, which requires ℓ = even for non-vanishing matrix elements; and (iii) $L = 2$ for *d*-electrons, which restricts ℓ to 0, 2 or 4 for non-vanishing matrix elements. Thus, the crystal-field Hamiltonian for the present problem contains only three terms.

$$H_{cf} = c_0 + c_2 Y_{20}(\theta) + c_4 Y_{40}(\theta). \tag{3}$$

These three crystal-field terms can be thought of as the electrostatic energy contribution to a 3*d*-hole on Ni^+ after averaging the cylindrically symmetric electric charge distribution of the hypothetical closed-shell NiX^- molecule over the *d*-orbital radial distribution. The first term gives only a constant energy offset, which can be chosen to correspond to the observed center of gravity of the electronic states of the d^9 manifold. The second and third terms are of greater interest, since they determine the splittings between the $^2\Sigma$, $^2\Pi$, and $^2\Delta$ electronic states.

Note that in the present work we treat the coefficients c_0, c_1, and c_2 as empirical parameters that are adjusted to fit experimental data. This is quite different from Refs. [28,29], where these parameters were computed by quantum chemistry methods, and then used to predict energy level positions and assignments.

The crystal-field Hamiltonian in Eq. (3) can be further simplified by using the concept of operator equivalents [35,39], which allows us, when only $\Delta L = 0$ matrix elements are considered (i.e., only matrix elements within the d^9 manifold), to avoid 3-*j* and 6-*j* symbols, etc. and simply replace the spherical harmonics by appropriate collections of orbital angular momentum operators. With this simplification, and with arbitrary scaling factors for the operator equivalents, H_{cf} becomes

$$H_{cf} = C_0 + C_2[(1/6)(3L_z^2 - \boldsymbol{L}^2)] + C_4[(1/48)(35L_z^4 - 30\boldsymbol{L}^2L_z^2 + 3\boldsymbol{L}^4 + 25L_z^2 - 6\boldsymbol{L}^2)]. \tag{4}$$

A convenient electronic basis set for use with $H_{non\text{-}rot} = H_{so} + H_{cf}$ can be written as [27–29]

$$|L, \Lambda\rangle|S, \Sigma\rangle, \tag{5}$$

where Λ and Σ represent the signed projections of $\boldsymbol{L}$ and $\boldsymbol{S}$, respectively, along the diatomic axis. Another electronic basis set, obtained by first coupling $\boldsymbol{L}$ and $\boldsymbol{S}$ to get the total electronic angular momentum $\boldsymbol{J_e} = \boldsymbol{L} + \boldsymbol{S}$ and then taking the signed projection $\Omega_e \equiv \Lambda + \Sigma$ of $\boldsymbol{J}_e$ along the diatomic axis, can be written as

$$|L, S; J_e, \Omega_e\rangle. \tag{6}$$

The basis set of Eq. (5) will always be used when setting up Hamiltonian matrices below, but the basis set of Eq. (6), which is more

closely related to the Ni^+ atomic $^2D_{3/2}$ and $^2D_{5/2}$ states (and sometimes more closely related to the final eigenfunctions) will often aid in our qualitative understanding.

It is now time to compare the number of parameters in $H_{non\text{-}rot}$ to the number of levels in the non-rotating molecule. There are four adjustable parameters in $H_{non\text{-}rot}$ as defined by Eqs. (1)–(4), namely A, C_0, C_2, and C_4. There are ten basis functions in Eq. (5) when $L = 2$ and $S = 1/2$, but because of symmetry (Section 2.7) these states all occur as doubly degenerate pairs in the non-rotating molecule, giving rise to only five energy levels. The result of this counting is thus somewhat disappointing, since the number of adjustable parameters is only one less than the number of energy levels for the d^9 manifold. If one could assume $|C_4| \ll |C_2|$, one of these parameters could be eliminated, but this assumption does not seem to be useful for the NiX series (Section 4).

2.2. Non-rotating-molecule Hamiltonian matrix and energy levels

Using well-known angular momentum matrix elements, it is relatively easy to set up the matrix of the Hamiltonian $H_{non\text{-}rot}$ in the basis set $|L, \Lambda\rangle|S, \Sigma\rangle$ [37]. Since $H_{non\text{-}rot}$ has no matrix elements off-diagonal in Ω_e, the non-rotating-molecule Hamiltonian matrix immediately factors into six submatrices, two of dimension 1, with $\Omega_e = \pm 5/2$, and four of dimension 2, with $\Omega_e = \pm 3/2$ and $\pm 1/2$. Because of symmetry, we need diagonalize only the matrices with positive values of Ω_e.

For $\Omega_e = +5/2$, the only element of the 1×1 Hamiltonian matrix is

$$\langle 2,+2|\langle 1/2,+1/2|H_{non-rot}|2,+2\rangle|1/2,+1/2\rangle = C_0 + A + C_2 + (1/4)C_4. \quad (7)$$

For $\Omega_e = +3/2$, the independent elements of the 2×2 Hermitian Hamiltonian matrix are

$$\langle 2,+2|\langle 1/2,-1/2|H_{non\text{-}rot}|2,+2\rangle|1/2,-1/2\rangle = C_0 - A + C_2 + (1/4)C_4, \quad (8a)$$

$$\langle 2,+1|\langle 1/2,+1/2|H_{non\text{-}rot}|2,+1\rangle|1/2,+1/2\rangle = C_0 + (1/2)A - (1/2)C_2 - C_4, \quad (8b)$$

$$\langle 2,+2|\langle 1/2,-1/2|H_{non\text{-}rot}|2,+1\rangle|1/2,+1/2\rangle = +A. \quad (8c)$$

For $\Omega_e = +1/2$, the independent elements of the 2×2 Hermitian Hamiltonian matrix are

$$\langle 2,+1|\langle 1/2,-1/2|H_{non\text{-}rot}|2,+1\rangle|1/2,-1/2\rangle = C_0 - (1/2)A - (1/2)C_2 - C_4, \quad (9a)$$

$$\langle 2,0|\langle 1/2,+1/2|H_{non\text{-}rot}|2,0\rangle|1/2,+1/2\rangle = C_0 - C_2 + (3/2)C_4, \quad (9b)$$

$$\langle 2,+1|\langle 1/2,-1/2|H_{non\text{-}rot}|2,0\rangle|1/2,+1/2\rangle = +(3/2)^{1/2}A. \quad (9c)$$

Matrix elements for the corresponding basis functions with $\Omega_e < 0$ can be obtained from Eqs. (7)–(9) by changing the signs of all Λ and Σ values on the left of the equalities. (Note that the matrix elements in Eqs. (7)–(9) agree, for example, with those in Ref. [28], apart from a change in notation.)

The matrices above can all be diagonalized algebraically to obtain the following non-rotating-molecule energy levels as a function of the spin–orbit coupling constant A and the three crystal-field parameters C_0, C_2, and C_4.

$$E(\Omega_e = +5/2) = C_0 + A + C_2 + (1/4)C_4, \quad (10a)$$

$$E_\pm(\Omega_e = +3/2) = C_0 + (1/4)\{[-A + C_2 - (3/2)C_4] \pm [25A^2 - 3A(6C_2 + 5C_4) + (1/4)(6C_2 + 5C_4)^2]^{1/2}\}, \quad (10b)$$

$$E_\pm(\Omega_e = +1/2) = C_0 + (1/4)\{(-A - 3C_2 + C_4) \pm [25A^2 - 2A(C_2 - 5C_4) + (C_2 - 5C_4)^2]^{1/2}\}, \quad (10c)$$

where the ± subscripts in Eqs. (10b) and (10c) indicate the higher and lower energy state for a given Ω_e. An identical set of levels is obtained for the corresponding negative values of Ω_e.

Let us now look at three limiting cases defined by the energies in Eq. (10). If $C_2 = C_4 = 0$, we recapture the Ni^+ atomic energy levels, i.e. $^2D_{3/2}$ at $C_0 - (3/2)A$ and $^2D_{5/2}$ at $C_0 + A$, although the $J_e = 3/2$ and 5/2 levels are only labeled in Eq. (10) by their Ω_e projections along the internuclear axis. When $A > 0$ the spin–orbit splitting is regular. When $A < 0$, as expected for a d-hole [38], it is inverted. If $A = C_4 = 0$ and $C_2 > 0$, Eq. (10) gives (again labeled only by their Ω_e projections) a case (b) $^2\Sigma$ ground state at $C_0 - C_2$, the two spin components of a case (b) $^2\Pi$ state at $C_0 - (1/2)C_2$, and the two components of a case (b) $^2\Delta$ state at $C_0 + C_2$. If $C_2 < 0$, the $^2\Delta$ state becomes the ground state. If $A = C_2 = 0$ and $C_4 > 0$, Eq. (10) gives a $^2\Sigma$ state at $C_0 + (3/2)C_4$, a $^2\Pi$ ground state at $C_0 - C_4$, and a $^2\Delta$ state at $C_0 + (1/4)C_4$. If $C_4 < 0$, the ground state is $^2\Sigma$.

It is also useful to look at how the four parameters in Eq. (10) are related to various sums of the observed electronic energy levels.

$$\begin{aligned} &E(+5/2) = C_0 + A + C_2 + (1/4)C_4, \\ &(1/2)[E_+(+3/2) + E_-(+3/2)] = C_0 + (1/4)[-A + C_2 - (3/2)C_4], \\ &(1/2)[E_+(+1/2) + E_-(+1/2)] = C_0 + (1/4)(-A - 3C_2 + C_4). \end{aligned} \quad (11)$$

Eq. (11) indicates that C_0 is the center of gravity of all five levels. It further shows that if A is fixed to some estimated value (presumably near the atomic Ni^+ value), then values for the three crystal-field parameters, including their signs, can be determined from a set of three linear equations.

2.3. Empirical correction factor β

The number of adjustable parameters could theoretically be increased by one, making it equal to the number of non-rotating-molecule energy levels in the $3d^9$ manifold, by noting that the spin–orbit interaction should be decomposed (on group-theoretical grounds) into one interaction along the diatomic axis and a slightly different interaction perpendicular to the diatomic axis, i.e.,

$$H_{so} = A_\parallel L_z S_z + A_\perp (L_x S_x + L_y S_y). \quad (12)$$

If the Ni^+ atomic d-orbital is not too badly distorted by molecule formation, we might hope that the introduction of this extra parameter would not be necessary for a reasonable description of the non-rotating-molecule energy levels.

In fact, after some trial and error, a slightly different empirical adjustment [27] seems helpful, as explained in more detail in Section 4. For matrix elements of the orbital angular momentum ladder operator we suppose

$$\langle 2,+2|L_+|2,+1\rangle = +2, \quad (13a)$$

$$\langle 2,+1|L_+|2,0\rangle = +\beta\sqrt{6}, \quad (13b)$$

with $0.5 \leqslant \beta \leqslant 1$. This is equivalent to the assumption [27] that the $|L = 2, \Lambda = \pm 2\rangle$ and $|L = 2, \Lambda = \pm 1\rangle$ electronic orbital functions are quite pure, but that $|L = 2, \Lambda = 0\rangle$ is significantly contaminated by

some unknown $|\Lambda = 0\rangle$ function from outside the $3d^9$ manifold. Eq. (13b) leads to altered Eqs. (9c) and (10c) of the form

$$\langle 2,+1|\langle 1/2,-1/2|H_{non\text{-}rot}|2,0\rangle|1/2,+1/2\rangle = +(3/2)^{1/2}\beta A, \quad (14a)$$

$$\begin{aligned} E_{\pm}(\Omega_e = +1/2) &= C_0 + (1/4)\{(-A - 3C_2 + C_4) \pm [(1 + 24\beta^2)A^2 \\ &\quad - 2A(C_2 - 5C_4) + (C_2 - 5C_4)^2]^{1/2}\}. \end{aligned} \quad (14b)$$

2.4. Rotating-molecule Hamiltonian operator and basis set

The rotating-molecule Hamiltonian can be written in the usual way [37], by multiplying the rotational constant B of the diatomic molecule by the square of the purely rotational angular momentum $\boldsymbol{R}$, to obtain

$$\begin{aligned} H_{rot} = B\boldsymbol{R}^2 &= B[(J_x - L_x - S_x)^2 + (J_y - L_y - S_y)^2] \\ &= B[\boldsymbol{J}^2 - J_z^2 + \boldsymbol{L}^2 - L_z^2 + \boldsymbol{S}^2 - S_z^2 + (L_+S_- + L_-S_+) \\ &\quad - (J_+L_- + J_-L_+) - (J_+S_- + J_-S_+)]. \end{aligned} \quad (15)$$

A quartic centrifugal distortion operator H_{cd} can be written as well, in the form

$$H_{cd} = -D\boldsymbol{R}^4 = -D[(J_x - L_x - S_x)^2 + (J_y - L_y - S_y)^2]^2. \quad (16)$$

The electronic-rotational basis set for the full Hamiltonian then takes one of the two forms

$$|L, \Lambda\rangle|S, \Sigma\rangle|J, \Omega\rangle, \quad (17a)$$

$$|L, S;\ J_e, \Omega_e\rangle|J, \Omega\rangle, \quad (17b)$$

where the $|J, \Omega\rangle$ are basically symmetric-top basis functions modified to eliminate one rotational angle [37], and where, as for all linear molecules (because $R_z \equiv 0$), we require [37]

$$\Omega \equiv \Omega_e = \Lambda + \Sigma. \quad (18)$$

2.5. Rotating-molecule Hamiltonian matrix elements with and without the empirical correction factor β

We now turn to the problem of calculating rotational energy levels for the electronic states belonging to a d^9 manifold. H_{rot} in Eq. (15) and H_{cd} in Eq. (16) have non-vanishing matrix elements off-diagonal in $\Omega \equiv \Omega_e$, so that matrices of dimension 10 must in principle be diagonalized to obtain the final rotational levels for all electronic states in the d^9 manifold. This is in fact what was done in the ^{2}D supermultiplet treatment of NiH in Ref. [27]. In the present paper, we instead calculate only rotational energy levels for $\Omega = 1/2$ states that are separated from other states by energies large compared to BJ. Such "isolated" $\Omega = 1/2$ states are expected to be the normal situation up to relatively high J values in the nickel halides. For NiH, on the other hand, the value of BJ approaches electronic state energy separations even for moderate J values, so that the full 10×10 matrix treatment cannot easily be avoided for transition metal hydrides.

The non-vanishing matrix elements of each part of H_{rot} in Eq. (15) in the basis set of Eq. (17a) are given by

$$\begin{aligned} &\langle L, \Lambda, S, \Sigma, J, \Omega|B[\boldsymbol{J}^2 - J_z^2 + \boldsymbol{L}^2 - L_z^2 + \boldsymbol{S}^2 - S_z^2]|L, \Lambda, S, \Sigma, J, \Omega\rangle \\ &\quad = +B[J(J+1) - \Omega^2 + L(L+1) - \Lambda^2 + S(S+1) - \Sigma^2], \end{aligned} \quad (19a)$$

$$\begin{aligned} &\langle L, \Lambda \pm 1, S, \Sigma \mp 1, J, \Omega|B(L_+S_- + L_-S_+)|L, \Lambda, S, \Sigma, J, \Omega\rangle \\ &\quad = +B[(L \mp \Lambda)(L \pm \Lambda + 1)(S \pm \Sigma)(S \mp \Sigma + 1)]^{1/2}, \end{aligned} \quad (19b)$$

$$\begin{aligned} &\langle L, \Lambda \pm 1, S, \Sigma, J, \Omega \pm 1| - B(J_+L_- + J_-L_+)|L, \Lambda, S, \Sigma, J, \Omega\rangle \\ &\quad = -B[(J \mp \Omega)(J \pm \Omega + 1)(L \mp \Lambda)(L \pm \Lambda + 1)]^{1/2}, \end{aligned} \quad (19c)$$

$$\begin{aligned} &\langle L, \Lambda, S, \Sigma \pm 1, J, \Omega \pm 1| - B(J_+S_- + J_-S_+)|L, \Lambda, S, \Sigma, J, \Omega\rangle \\ &\quad = -B[(J \mp \Omega)(J \pm \Omega + 1)(S \mp \Sigma)(S \pm \Sigma + 1)]^{1/2}. \end{aligned} \quad (19d)$$

We also give matrix elements for the sum of the operators in Eqs. (19c) and (19d) in the basis set of Eq. (17b)

$$\begin{aligned} &\langle L,S;J_e,\Omega_e \pm 1;J,\Omega \pm 1| - B[J_+(L_- + S_-) + J_-(L_+ + S_+)]|L,S;J_e,\Omega_e;J,\Omega\rangle \\ &\quad = -B[(J \mp \Omega)(J \pm \Omega + 1)(J_e \mp \Omega_e)(J_e \pm \Omega_e + 1)]^{1/2}, \end{aligned} \quad (20)$$

since this expression will be convenient when discussing molecule formation from the X^- and $^2D_{3/2}$ or $^2D_{5/2}$ Ni^+ separated ion limits [34].

The question now arises of how to introduce the empirical correction factor β into the rotating-molecule problem in a way that is consistent with its introduction into the non-rotating-molecule problem. It seems obvious that we must again use β so that $\langle \Lambda = \pm 1|L_{\pm}|\Lambda = 0\rangle = \langle \Lambda = 0|L_{\mp}|\Lambda = \pm 1\rangle \rightarrow +\beta\sqrt{6}$, i.e., we must replace Eqs. (19b) and (19c) above, when $\Lambda = 0$, by

$$\begin{aligned} &\langle L, \pm 1, S, \Sigma \mp 1, J, \Omega|B(L_+S_- + L_-S_+)\ |\ (L, 0, S, \Sigma, J, \Omega\rangle \\ &\quad = +\beta B[L(L+1)(S \pm \Sigma)(S \mp \Sigma + 1)]^{1/2}, \end{aligned} \quad (21a)$$

$$\begin{aligned} &\langle L, \pm 1, S, \Sigma, J, \Omega \pm 1| - B(J_+L_- + J_-L_+)|(L, 0, S, \Sigma, J, \Omega\rangle \\ &\quad = -\beta B[(J \mp \Omega)(J \pm \Omega + 1)L(L+1)]^{1/2}. \end{aligned} \quad (21b)$$

Since the quantum number Λ is not present in the basis set of Eq. (17b), it is not easy to introduce this correction factor into Eq. (20).

2.6. Rotating-molecule energies for $|\Omega_e| = 1/2$ states

Because of various possibilities for confusion in this section, we distinguish more carefully than usual between signed values Ω and unsigned values $|\Omega|$ for this quantum number, as well as between the projection along the diatomic (or linear) axis Ω_e of the electronic (or vibronic) angular momentum $\boldsymbol{J}_e$ and the projection Ω along this same axis of the total angular momentum $\boldsymbol{J}$ (even though $\Omega_e \equiv \Omega$ for linear molecules).

We are particularly interested in the rotational energy levels of the $|\Omega_e| = 1/2$ states in the $3d^9$ manifold, because these two states normally exhibit very large Ω-type doubling. We make the further assumption in this section that the two $|\Omega_e| = 1/2$ states are well separated from each other and from other $|\Omega_e|$ states, i.e., separated by energies large compared to BJ. It is then useful, as shown below, to imagine a continuum of properties for this pair of $|\Omega_e| = 1/2$ states. At one limit we have the familiar rotational levels of a case (a) $^2\Pi_{1/2}$ state and a case (b) $^2\Sigma$ state, corresponding to $\Omega_e = \pm 1/2$ non-rotating-molecule wavefunctions of the form $|\Lambda = \pm 1, \Sigma = \mp 1/2\rangle$ and $|\Lambda = 0, \Sigma = \pm 1/2\rangle$, respectively. At the other limit we have the relatively unfamiliar rotational levels of a $J_e = 3/2$, $|\Omega_e| = 1/2$ state and a $J_e = 5/2$, $|\Omega_e| = 1/2$ state, corresponding to $\Omega_e = \pm 1/2$ wavefunctions of the form $0.775|\Lambda = \pm 1,\ \Sigma = \mp 1/2\rangle - 0.632|\Lambda = 0,\ \Sigma = \pm 1/2\rangle$ and $0.632|\Lambda = \pm 1,\ \Sigma = \mp 1/2\rangle + 0.775|\Lambda = 0,\ \Sigma = \pm 1/2\rangle$, respectively.

Because a case (b) $^2\Sigma$ state exists at only one point along this continuum of wavefunctions, we choose here to use always the $|\Omega_e| = 1/2$ state expression for Ω-type doubling [34]

$$E_{rot}(|\Omega_e| = 1/2) = BJ(J+1) \pm (1/2)p(J + 1/2), \quad (22)$$

where J is half-integral, rather than the $^2\Sigma$ expressions for rho-type doubling [34]

$$E_{rot}(^2\Sigma) = BN(N+1) + (1/2)\gamma N, \quad (23a)$$

$$E_{rot}(^2\Sigma) = BN(N+1) - (1/2)\gamma(N+1), \quad (23b)$$

where N is integral and Eqs. (23a) and (23b) apply to $J = N + 1/2$ and $J = N - 1/2$, respectively. In fact, Eqs. (22) and (23) describe the

same set of rotational energy levels from two different points of view, so they can be interconverted, but the exact process depends on the sign conventions adopted for p in Eq. (22), as discussed in Section 2.7, and on whether the $^2\Sigma$ state is a $^2\Sigma^+$ or a $^2\Sigma^-$ state.

Although the details of the physical interactions in the molecules are quite different, matrix elements like those in Eqs. (19) have been successfully used in the past to explain anomalously large spin-rotation splittings in several types of $|\Omega_e| = 1/2$ states. The procedure has two steps. In the first step, the composition of a given pair of degenerate non-rotating-molecule $|\Omega_e = \pm 1/2\rangle$ states (in some appropriate basis set for the non-rotating molecule) is either assumed or determined experimentally. In the second step, matrix elements of H_{rot} are calculated between the rotating-molecule wavefunctions $|\Omega_e = +1/2\rangle|J, \Omega = +1/2\rangle$ and $|\Omega_e = -1/2\rangle|J, \Omega = -1/2\rangle$ corresponding to these states. In one example of this procedure [40], the compositions of the two $^2\Sigma$ vibronic states arising for $v_2 = 1$ in a linear triatomic molecule exhibiting the Renner–Teller effect were calculated from the spin–orbit coupling constant and the Renner–Teller parameter, after which $\Delta\Sigma = \pm 1$ matrix elements of the type in Eq. (19d) were used to compute the Ω-type doubling parameter p. In another example [41], the non-rotating molecule $|\Omega_e = \pm 1/2\rangle$ states were assumed to have the $\Lambda = 0$, $\Sigma = \pm 1/2$ composition appropriate for a pure $^{2S+1}\Sigma$ state of a diatomic molecule, but the 1/2 states were assumed to be well separated (because of large second-order spin–orbit effects) from the other components of the $^{2S+1}\Sigma$ state so that matrix elements of H_{rot} between the $\Omega_e = \pm 1/2$ pair and other states could be ignored. Fig. 1 of Ref. [41] presents a diagram showing how the $p \leftrightarrow \gamma$ conversion process works for $^{2S+1}\Sigma^{\pm}$ states and for one choice of sign conventions for p. In a third example, matrix elements like those in Eq. (20) have been used to explain the large spin-rotation splitting in an excited electronic state of $HgAr^+$ [42,43] that correlates with the separated atoms $Hg^+(^2D_{5/2}) + Ar(^1S_0)$. This $HgAr^+$ situation is actually quite similar to the problem under discussion here, since some of the $3d^9$ states of NiX can be correlated with $Ni^+(^2D_{5/2}) + X^-(^1S_0)$.

A general calculation, appropriate for rotational levels of the two $|\Omega_e| = 1/2$ states in a d^9 manifold, can be carried out as follows. The 2×2 Hamiltonian matrix for the non-rotating molecule is set up using Eqs. (9a), (9b), and (14a). The required algebraic calculation can be simplified by formally defining two new variables r and θ (as functions of A, C_0, C_2, and C_4), so that the matrix implied by Eqs. (9a), (9b), and (14a) has the form

$$\begin{bmatrix} H_0 + r\cos 2\theta & +r\sin 2\theta \\ +r\sin 2\theta & H_0 - r\cos 2\theta \end{bmatrix}. \tag{24}$$

In this matrix, row 1 and column 1 are labeled by $|L, \Lambda\rangle|S, \Sigma\rangle = |2, +1\rangle|1/2, -1/2\rangle$, and row 2 and column 2 by $|L, \Lambda\rangle|S, \Sigma\rangle = |2, 0\rangle|1/2, +1/2\rangle$, and also

$$\begin{aligned} H_0 &= C_0 + (1/4)(-A - 3C_2 + C_4), \\ r\cos 2\theta &= (1/4)(-A + C_2 - 5C_4), \\ r\sin 2\theta &= +\beta(3/2)^{1/2}A, \end{aligned} \tag{25}$$

with r always taken to be positive. Note that Eqs. (24) and (25) also describe the Hamiltonian matrix obtained when row and column 1 are labeled by $|L, \Lambda\rangle|S, \Sigma\rangle = |2, -1\rangle|1/2, +1/2\rangle$, and row and column 2 by $|L, \Lambda\rangle|S, \Sigma\rangle = |2, 0\rangle|1/2, -1/2\rangle$.

The column eigenvectors and their eigenvalues from the matrix in Eq. (24) can then be written rather simply in terms of r and θ as

$$\begin{matrix} \begin{bmatrix} +\cos\theta \\ +\sin\theta \end{bmatrix} & \begin{bmatrix} -\sin\theta \\ +\cos\theta \end{bmatrix}, \\ H_0 + r & H_0 - r \\ \Psi_{\Omega_e}(2) & \Psi_{\Omega_e}(1) \end{matrix} \tag{26}$$

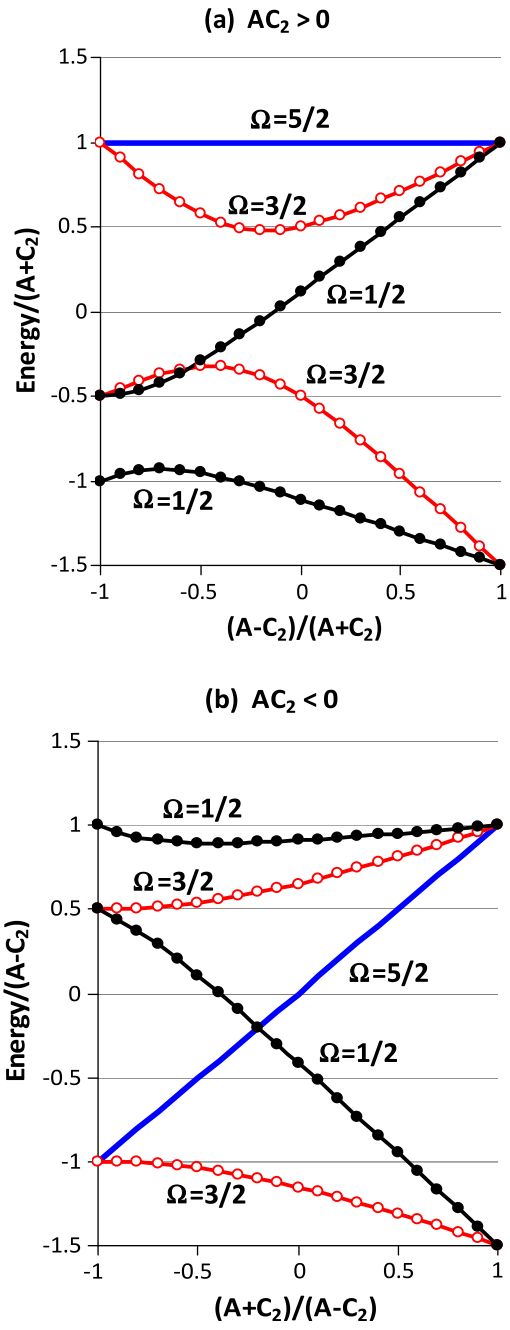

Fig. 1. Reduced electronic energy levels (unitless) for a d^9 manifold in NiX, calculated from Eqs. (10a)–(10c) with $C_4 = 0$, and plotted against a ratio (unitless) involving the spin–orbit coupling constant A in Eq. (2) and the crystal-field parameter C_2 in Eq. (4). Energies for the two $\Omega = 1/2$ states are plotted as solid circles –●–. Energies for the two $\Omega = 3/2$ states are plotted as open circles –○–. Energies for the $\Omega = 5/2$ state are plotted as a solid line. Note that spin–orbit coupling is absent at the extreme left of these diagrams, so that the three energy levels there are those of a Hund's case (b) $^2\Sigma$, $^2\Pi$, and $^2\Delta$ state. Crystal-field interaction is absent at the extreme right, so that the two energy levels there are those of an atomic $^2D_{3/2}$ and $^2D_{5/2}$ state. (a) Energy levels when A and C_2 have the same sign. If both constants are positive (negative), the sign on the ordinate labels is the same as (opposite to) the sign of the true energy. (b) Energy levels when A and C_2 have opposite sign. If $A - C_2$ is positive (negative), the sign on the ordinate labels is the same as (opposite to) the sign of the true energy. The differences in Fig. 1a and b mainly arise from the fact that the energy level patterns on the left in these two diagrams are the negatives of each other, while the patterns on the right are exactly the same.

for either $\Omega_e = +1/2$ or $-1/2$. The (1), (2) labels on the wavefunctions $\Psi_{\Omega e}$ follow the convention of counting states of the same symmetry from the lowest energy state upward. Note that there is an arbitrary

sign in Eq. (26). If, for example, 2θ is replaced by $2\theta - 2\pi$ in Eq. (25), then θ is replaced by $\theta - \pi$ in Eq. (26). This changes the sign of both $\cos\theta$ and $\sin\theta$, corresponding to a multiplication of the original $\Psi_{\Omega e}(1)$ and $\Psi_{\Omega e}(2)$ wavefunctions by the arbitrary phase factor -1.

We now set up the 2×2 matrix of H_{rot} within electronic-rotational basis functions formed by multiplying the electronic functions in Eq. (26) by appropriate $|J, \Omega\rangle$ rotational functions. Consider first the matrix whose rows and columns are labeled by $\Omega = \pm 1/2$ electronic-rotational basis functions formed from the higher-energy electronic functions $\Psi_{+1/2}(2)$ and $\Psi_{-1/2}(2)$ from Eq. (26), i.e., the matrix whose rows and columns are labeled (in the notation $|L, \Lambda\rangle|S, \Sigma\rangle|J, \Omega\rangle$) by

$$\Psi_{+1/2}(2)|J,+1/2\rangle = +\cos\theta|2,+1\rangle|1/2,-1/2\rangle|J,+1/2\rangle + \sin\theta|2,0\rangle|1/2,+1/2\rangle|J,+1/2\rangle, \quad (27a)$$

$$\Psi_{-1/2}(2)|J,-1/2\rangle = +\cos\theta|2,-1\rangle|1/2,+1/2\rangle|J,-1/2\rangle + \sin\theta|2,0\rangle|1/2,-1/2\rangle|J,-1/2\rangle. \quad (27b)$$

Matrix elements from the parts of H_{rot} in Eq. (19a) and in Eq. (19b), which is in fact replaced by Eq. (21a), are diagonal in this basis set, with the same value in both diagonal positions of the 2×2 matrix:

$$\begin{aligned} &B\cos^2\theta[J(J+1) - (1/2)^2 + 6 - 1^2 + 3/4 - (1/2)^2] \\ &\quad + B\sin^2\theta[J(J+1) - (1/2)^2 + 6 - 0^2 + 3/4 - (1/2)^2] \\ &\quad + 2\sqrt{6}\beta B\sin\theta\cos\theta \\ &= B[J(J+1) + 23/4] - (1/2)B\cos 2\theta + \sqrt{6}\beta B\sin 2\theta. \end{aligned} \quad (28)$$

Matrix elements from the parts of H_{rot} in Eq. (19c), which is replaced by Eq. (21b), and in Eq. (19d) are off-diagonal in the basis set of $\Psi_{+1/2}(2)\ |J,+1/2\rangle$ and $\Psi_{-1/2}(2)\ |J,-1/2\rangle$, with the same value in both off-diagonal positions of the 2×2 matrix:

$$\begin{aligned} &-B(J+1/2)[(1/2)(1-\cos 2\theta) + \sqrt{6}\beta\sin 2\theta] \\ &\quad \equiv +(1/2)p_{(2)}(J+1/2). \end{aligned} \quad (29)$$

The off-diagonal element of H_{rot} is equated on the right of Eq. (29) to the usual splitting expression for $|\Omega_e| = 1/2$ states, with a subscript (2) on p to indicate that this is the p value associated with the higher-energy $|\Omega_e| = 1/2$ state. The plus sign used in this definition of $p_{(2)}$ will be explained in the next section, where e and f levels and parity are discussed.

Equations analogous to Eqs. (28) and (29) can be obtained for electronic-rotational basis functions formed from the lower-energy electronic functions $\Psi_{+1/2}(1)$ and $\Psi_{-1/2}(1)$ in Eq. (26) by making the formal substitution $\theta \to \theta + \pi/2$. We then obtain for the diagonal element

$$B[J(J+1) + 23/4] + (1/2)B\cos 2\theta - \sqrt{6}\beta B\sin 2\theta, \quad (30)$$

and for the off-diagonal element

$$\begin{aligned} &-B(J+1/2)[(1/2)(1+\cos 2\theta) - \sqrt{6}\beta\sin 2\theta] \\ &\quad \equiv +(1/2)p_{(1)}(J+1/2). \end{aligned} \quad (31)$$

Consider now these Ω-type doubling results for two limiting cases. For the first limiting case, we take $C_2 - 5C_4 \gg |A| \gg BJ$, so that crystal-field effects are much larger than spin–orbit effects. This leads to the limiting values $\cos 2\theta = +1$ and $\sin 2\theta = 0$ in Eq. (25). Substituting these values into Eqs. (28)–(31), and diagonalizing the implicit 2×2 matrix, we obtain the following J-dependent part of the energy level expressions for the upper ($^2\Pi$) and lower ($^2\Sigma$) $\Omega = 1/2$ states, respectively

$$E_{rot}(^2\Pi) = BJ(J+1), \quad (32a)$$

$$E_{rot}(^2\Sigma) = BJ(J+1) \pm B(J+1/2), \quad (32b)$$

where as always in this paper, J is half-integral. Eq. (32a) gives the rotational energy levels of a case (a) $^2\Pi_{1/2}$ state that exhibits no Ω-type doubling. Eq. (32b) can be converted in the usual way [37] to the familiar $BN(N+1)$ rotational energy levels of a case (b) $^2\Sigma$ state (where N is an integer) by making the substitution $J + 1/2 \to N$ for the upper sign choice and $J - 1/2 \to N$ for the lower sign choice.

For the second limiting case we take $|A| \gg |C_2|, |C_4| \gg BJ$, with $A < 0$ and $\beta = 1$, so that spin–orbit effects are much larger than crystal-field effects. This leads to the limiting values $\cos 2\theta = +(1/5)$ and $\sin 2\theta = -(24/25)^{1/2}$ in Eq. (25). Substituting these values into Eq. (28)–(31) and diagonalizing, we obtain for the upper ($^2D_{3/2}$) and lower ($^2D_{5/2}$) $|\Omega_e| = 1/2$ states

$$E_{rot}(^2D_{3/2}) = BJ(J+1) \pm 2B(J+1/2), \quad (33a)$$

$$E_{rot}(^2D_{5/2}) = BJ(J+1) \pm 3B(J+1/2), \quad (33b)$$

where Eq. (33b) agrees with the results for $HgAr^+$ in Ref. [42].

2.7. Parity considerations

There is a recommended convention [44] for labeling rotational states of different parity [34,37] in linear molecules with an odd number of electrons, namely e states have parity $+(-1)^{J-1/2}$ and f states have parity $-(-1)^{J-1/2}$. Following the sign convention for p in widespread use for the nickel halides [4,6,9,13], we then write

$$F_e(J) = BJ(J+1) + (1/2)p(J+1/2), \quad (34a)$$

$$F_f(J) = BJ(J+1) - (1/2)p(J+1/2). \quad (34b)$$

While not specifically discussed here, phase conventions for the various basis functions have been chosen so that they transform as follows [37] under the parity operator σ_v (recall that the laboratory-fixed inversion operation E^* used to define the parity of a state corresponds in molecule-fixed coordinates to reflection σ_v in a plane containing the diatomic axis [37]),

$$\begin{aligned} &\sigma_v|L,\Lambda\rangle = (-1)^{L-\Lambda}|L,-\Lambda\rangle, \\ &\sigma_v|S,\Sigma\rangle = (-1)^{S-\Sigma}|S,-\Sigma\rangle, \\ &\sigma_v|J,\Omega\rangle = (-1)^{J-\Omega}|J,-\Omega\rangle, \\ &\sigma_v|L,\Lambda\rangle|S,\Sigma\rangle|J,\Omega\rangle = (-1)^{J-1/2}|L,-\Lambda\rangle|S,-\Sigma\rangle|J,-\Omega\rangle, \end{aligned} \quad (35)$$

where we have used $L = 2$, $S = 1/2$, and $\Lambda + \Sigma + \Omega = 2\Omega =$ odd integer to simplify the last equation. Eq. (35) can be used to show that the two electronic-rotational basis functions in Eqs. (27a) and (27b) are related by

$$\sigma_v\Psi_{+1/2}(2)|J,+1/2\rangle = (-1)^{J-1/2}\Psi_{-1/2}(2)|J,-1/2\rangle, \quad (36)$$

with a similar equation relating the electronic-rotational basis functions formed from $\Psi_{+1/2}(1)$ and $\Psi_{-1/2}(1)$ in Eq. (26). Eq. (36) indicates that $\Psi_{+1/2}(2)|J,+1/2\rangle + \Psi_{-1/2}(2)\ |J,-1/2\rangle$ is an e function, and $\Psi_{+1/2}(2)\ |J,+1/2\rangle - \Psi_{-1/2}(2)|J,-1/2\rangle$ is an f function. It is then a simple matter to note that the e function receives an energy contribution equal in sign and magnitude to the off-diagonal matrix element, while the f function receives an energy contribution equal to the negative of the off-diagonal matrix element. Comparison with Eq. (34) then requires the plus sign on the right of Eqs. (29) and (31).

The splitting parameters $p_{(1)}$ and $p_{(2)}$ for the two $|\Omega_e| = 1/2$ states in the d^9 configuration of NiX molecules, when signed according to these symmetry-based conventions, satisfy the following relations

$$p_{(1)} + p_{(2)} = -2B, \tag{37a}$$

$$p_{(1)} - p_{(2)} = -2B(2\sqrt{6}\beta \sin 2\theta - \cos 2\theta). \tag{37b}$$

Eq. (37a) gives a simple way of estimating p for one of the $\Omega_e = 1/2$ states, if p for the other $\Omega_e = 1/2$ state is known. Eq. (37b) can be used to show that the difference in signed p values for the two $\Omega_e = 1/2$ states falls between two limits, i.e.

$$-10B \leqslant -2B(1 + 24\beta^2)^{1/2} \leqslant (p_{(1)} - p_{(2)}) \leqslant +2B(1 + 24\beta^2)^{1/2} \leqslant +10B. \tag{38}$$

The existence of Kramers degeneracy for Ω_e = half-integral states in a non-rotating linear molecule like NiX can be derived from the transformation properties in Eq. (35), which are associated with reflection in a plane containing the linear axis. A consideration of time reversal, which is required to derive Kramers degeneracy in polyatomic molecules with no point-group symmetry, can be avoided in this paper.

3. Pictorial representation of electronic energy level patterns in the non-rotating molecule

The effects of the competition between crystal-field effects and spin–orbit effects in non-rotating NiX molecules can be illustrated by a simple diagram if we reduce the number of crystal-field splitting parameters from two to one by considering one of the idealized cases: (i) $C_4 \equiv 0$, (ii) $C_2 \equiv 0$, or (iii) $C_2/C_4 \equiv$ constant. For brevity we consider only the first case here. The general scheme is to first define two limiting cases, one with no spin–orbit interaction ($A = 0$) and one with no crystal-field interaction ($C_2 = 0$), and then to define intermediate cases using values of the unitless parameter $(A - C_2)/(A + C_2)$ when $AC_2 > 0$, or values of $(A + C_2)/(A - C_2)$ when $AC_2 < 0$. These ratios take values lying between -1 and $+1$ for all possible values of A and C_2 satisfying the indicated relative sign requirements.

Fig. 1a and b shows reduced energy levels (unitless) for the five spin–orbit components arising from the d^9 configuration, as obtained by dividing results calculated from Eq. (10) by $(A + C_2)$ when $AC_2 > 0$ or by $(A - C_2)$ when $AC_2 < 0$, respectively. At the left we have the Hund's case (b) $^2\Sigma$, $^2\Pi$, and $^2\Delta$ diatomic-molecule states. At the right we have the $^2D_{3/2}$ and $^2D_{5/2}$ atomic states. In between we have the molecular states arising when both spin–orbit and crystal-field effects are present. It can be seen that the energy ordering of the electronic states in Fig. 1 changes significantly on going from left to right in Fig. 1a and b, i.e., on going from the limiting case of no spin–orbit interaction to the limiting case of no crystal-field interaction.

Fig. 1a and b, and others like them, illustrate how one might attempt to use Eqs. (10a)–(10c) to discuss some part of the changes in the relative energy pattern for the five spin–orbit components arising from the $3d^9$ configuration across the four nickel halides (including changes in the ground state symmetry species) in terms of changes in electrostatic crystal-field effects, rather than discussing them exclusively in terms of changes in the *d*-electron participation in the molecular bonding.

4. Comparison with experiment

We now use the formulas derived above to treat the rather complete experimental spectral information on NiF and NiCl. For each molecule, the positions of the five electronic-state spin–orbit components will be treated first, and the Ω-doubling parameters for the $\Omega = 1/2$ states will be treated second.

4.1. NiF electronic energy levels

Columns 1 and 2 of Table 1 give state labels and positions in cm^{-1} for the five $3d^9$ spin–orbit components of NiF taken directly from Table 2 of Ref. [3]. Column 3 gives observed-minus-calculated residuals from a least-squares fit of these levels to the four parameters A, C_0, C_2, and C_4, using the expressions in Eq. (10). These residuals are quite large and evenly distributed among the five levels. Column 7 gives the parameter values obtained from this fit. The spin–orbit constant A is poorly determined and somewhat smaller in magnitude than that of the free Ni^+ ion.

Column 4 gives residuals from an exploratory (and in retrospect diagnostic) fit of the five levels to the three crystal-field parameters C_0, C_2, and C_4, with the spin–orbit constant fixed to its value in the free Ni^+ ion, as shown in column 8. Residuals from this fit suggest that something may be wrong with the treatment of the $\Omega = 1/2$ states. A visual display of this problem is presented in Fig. 2. Comparison of column 4 in Fig. 2, which shows the energy levels calculated from this exploratory fit, with the observed levels shown in column 6 indicates that the two $\Omega = 1/2$ states have been "pushed apart" too far by the theoretical model. Eq. (9c) indicates that the two $\Omega = 1/2$ basis functions are connected by an off-diagonal matrix element $+(3/2)^{1/2}A$, which takes the value $-738\ cm^{-1}$ when the Ni^+ value for A is used. This off-diagonal matrix element requires the two $\Omega = 1/2$ states calculated from the model to be

Table 1
Positions of the five spin–orbit components arising from the $3d^9$ ground electronic configuration in NiF, together with residuals and parameter values from three least-squares fits of these levels. All quantities are in cm^{-1}, except for β, which is unitless.

State[a]	T_0[b]	o–c[c]	o–c[d]	o–c[e]	Const[f]	Value[c]	Value[d]	Value[e]
$A^2\Delta_{3/2}$	2223.5743	44	5	6	A	−574(47)	−602.8[g]	−602.8[g]
$B^2\Sigma^+$	1574.1057	−34	−72	2	β	1.0[g]	1.0[g]	0.878[g]
$A^2\Delta_{5/2}$	829.4761	−34	−3	−4	C_0	976(48)	976(40)	976(3)
$^2\Sigma$	251.2522	67	94	0	C_2	392(66)	391(55)	386(4)
$X^2\Pi_{3/2}$	0	−43	−25	−3	C_4	282(88)	273(70)	300(5)

[a] In the notation of Table 2 of Ref. [3]. In the present work, we use only the Ω values to label these states, since Ω is a good quantum number in the non-rotating molecule, while Λ and Σ are not. $\Omega = 1/2$ for the two $^2\Sigma$ states in this column.
[b] In cm^{-1} from Table 2 of Ref. [3].
[c] Observed-minus-calculated residuals and parameter values from a fit to the four parameters A, C_0, C_2, and C_4 in Eq. (10). The A value obtained in this fit is very poorly determined, but still within one standard error of $A = -602.8\ cm^{-1}$ [33] in the free Ni^+ ion.
[d] Residuals and parameters from a fit to the three parameters C_0, C_2, and C_4 in Eq. (10), with A fixed to its free Ni^+ value. In this fit the most serious fitting problems occur for the two $\Omega = 1/2$ states (see text).
[e] Residuals and parameters from a fit to the three parameters C_0, C_2, and C_4 in Eqs. (10) and (14), where A has been fixed to its free Ni^+ value and the empirical correction factor β has been optimized manually to the nearest 0.001. In this fit the residuals are all below $10\ cm^{-1}$, which can be taken as an estimate of the accuracy for the simple model of this paper.
[f] Parameters from the energy expressions in Eqs. (10) and (14). Numbers in parentheses indicate one standard error (type A, $k = 1$) [45] from the least-squares fit.
[g] Parameter held fixed during the least-squares fit.

Table 2
Positions of the five spin–orbit components arising from the $3d^9$ ground electronic configuration in NiCl, together with residuals and parameter values from three least-squares fits of these levels. All quantities are in cm^{-1}, except for β, which is unitless.

State[a]	T_0[b]	o–c[c]	o–c[d]	o–c[e]	Const[f]	Value[c]	Value[d]	Value[e]
$B^2\Sigma^+$	1768	−30	−49	2	A	−587(39)	−602.8[g]	−602.8[g]
$A^2\Delta_{3/2}$	1646	31	7	8	β	1.0[g]	1.0[g]	0.897[g]
$X^2\Pi_{1/2}$	382	59	74	0	C_0	791(40)	791(31)	791(4)
$A^2\Delta_{5/2}$	161	−17	−0	−6	C_2	−85(56)	−84(43)	−88(5)
$X^2\Pi_{3/2}$	0	−43	−32	−5	C_4	234(75)	228(54)	263(6)

[a] In the notation of Fig. 1 of Ref. [10]. In the present work, we use only the Ω values to label these states, since they are good quantum numbers in the non-rotating molecule, while Λ and Σ are not. $\Omega = 1/2$ for the $^2\Sigma^+$ state in this column.
[b] In cm^{-1} from Fig. 1 of Ref. [10].
[c] Observed-minus-calculated residuals and parameter values from a fit to the four parameters A, C_0, C_2, and C_4 in Eqs. (10). The value of $A = -587(39)\ cm^{-1}$ obtained in this fit is very poorly determined, but still within one standard error of $A = -602.8\ cm^{-1}$ [33] in the free Ni^+ ion.
[d] Residuals and parameter values from a fit to the three parameters C_0, C_2, and C_4 in Eqs. (10), with A fixed to its value of $-602.8\ cm^{-1}$ in the free Ni^+ ion. In this fit the most serious fitting problems occur for the two $\Omega = 1/2$ states (see text).
[e] Residuals and parameter values from a fit to the four parameters β, C_0, C_2, and C_4 in Eqs. (10) and (14), where A has been fixed to its free Ni^+ value and the empirical correction parameter β has been optimized manually to the nearest 0.001. In this fit the residuals are all below $10\ cm^{-1}$, which can be taken as an estimate of the limit of accuracy for this simple model.
[f] Parameters from the energy expressions in Eqs. (10) and (14). Numbers in parentheses indicate one standard error (type A, $k = 1$) [45] from the least-squares fit.
[g] Parameter held fixed during the least-squares fit.

separated by at least $1476\ cm^{-1}$, when in fact the experimentally observed separation in NiF is only $1323\ cm^{-1}$. Attempts to fix this disagreement by starting the four-parameter fits with smaller values of A, in the hopes of finding another least-squares minimum in parameter space, were unsuccessful, e.g., fits starting with $A = -200\ cm^{-1}$, $-300\ cm^{-1}$, and $-400\ cm^{-1}$ all converged to the previously obtained fit shown in columns 3 and 7 of Table 1.

After some trial and error, it became clear that that the large residuals could be reduced by introducing the empirical correction factor β discussed in Section 2.3, which corresponds physically [27] to assuming that the $|L = 2, \Lambda = 0\rangle$ basis function in the $3d^9$ configuration is contaminated by orbital functions from other configurations. This assumption agrees well with the ab initio results reported in Table 3 of Ref. [31], i.e., (in their notation) "the δ_1 and π_1 molecular orbitals are essentially atomic Ni3*d*, whereas both σ_1 and σ_2 are hybrids between Ni3d_σ and Ni4*s*." Columns 5 and 9 of Table 1 show that all residuals can be reduced to $6\ cm^{-1}$ or less with A fixed to $-602.8\ cm^{-1}$ and β optimized manually to 0.878. This probably indicates the limit of accuracy that can be obtained from the present simple model. We note in passing, that if both A and β are floated, we then arrive at a (somewhat meaningless) exact fit of five lines to five parameters. Nevertheless, even this exact fit is encouraging, because it gives the physically reasonable values of $A = -606.9144\ cm^{-1}$ and $\beta = 0.87367$. We further note that these values for β in NiF are quite close to the value $c_{\Sigma\pi} = 0.855$ for the corresponding parameter in NiH, given in Table 5 of Ref. [27].

We now return to a closer examination of Fig. 2 (which is quite similar in design to Fig. 3 of Ref. [32]). The first column on the left gives the (hypothetical) energy of the ^2D state of the Ni^+ ion when spin–orbit interaction is removed, and when the zero of energy is placed at the position of the $\Omega = 3/2$ molecular ground state, shown further to the right in the diagram. This ^2D level is ten-fold degenerate. The second column from the left gives the (again hypothetical) energies of the $^2\Sigma$, $^2\Pi$, $^2\Delta$ states of NiF calculated when only the crystal-field interaction is turned on, i.e., calculated from the values of C_0, C_2, C_4 given in column 8 of Table 1 and a value of $A = 0$. Because $A = 0$, these can be thought of as the calculated positions of the Hund's case (b) electronic states arising from the $3d^9$

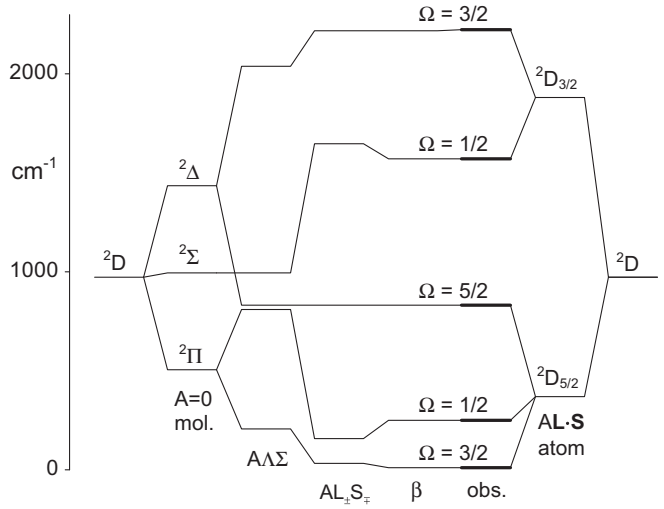

Fig. 2. Energy levels of NiF calculated when various interactions in Eqs. (10) and (14) are "turned on" sequentially. The first column on the left (column 1) gives the energy of the ten-fold degenerate ^2D state of the Ni^+ ion when spin–orbit interaction is suppressed. Column 2 gives the energies of the Hund's case (b) $^2\Sigma$, $^2\Pi$, $^2\Delta$ states of NiF calculated when only the crystal-field interaction is turned on (using C_0, C_2, C_4 from column 8 of Table 1 and $A = 0$). Column 3 gives the energies of the case (a) $^2\Sigma$, $^2\Pi_{1/2}$, $^2\Pi_{3/2}$, $^2\Delta_{3/2}$, and $^2\Delta_{5/2}$ states calculated when the crystal-field interaction and the diagonal spin–orbit interaction is turned on (using the same C_0, C_2, C_4 as before and $A = -602.8\ cm^{-1}$ in the operator AL_zS_z). Column 4 gives the case (c) energy levels calculated when the crystal-field interaction and the full spin–orbit interaction are turned on, i.e., using the previous constants and $A = -602.8\ cm^{-1}$ in the operator $A(L_xS_x + L_yS_z)$, corresponding to the fit summarized in columns 4 and 8 of Table 1. Column 5 gives the energy levels calculated in the least-squares fit summarized in columns 5 and 9 of Table 1, where both the crystal-field interaction and the full spin–orbit interaction are turned on, and where the matrix element between $\Lambda = 0$ and $\Lambda = \pm1$ is reduced, as shown in Eq. (21b), by an empirical factor $\beta = 0.878$. Disagreements between the calculated levels in column 5 and the observed levels [3] in column 6 (the thick lines) are almost invisible on the $2000\ cm^{-1}$ scale of this figure. The second column from the right in Fig. 2 shows the $^2D_{3/2}$ and $^2D_{5/2}$ energy levels of the free Ni^+ ion. The pattern of observed $3d^9$ electronic levels for NiF in column 6 can thus be viewed either as arising from crystal-field splittings of the Ni^+ atomic ion levels in column 7, or from spin–orbit splittings of the case (b) diatomic levels in column 2.

electron configuration in NiF. (It is important to remember, however, that the crystal-field constants used in this calculation were actually obtained when the spin–orbit constant A was fixed to $-602.8\ cm^{-1}$). The third column from the left gives the (again hypothetical) energies of the $^2\Sigma$, $^2\Pi_{1/2}$, $^2\Pi_{3/2}$, $^2\Delta_{3/2}$, and $^2\Delta_{5/2}$ states of NiF calculated when the crystal-field interaction and the diagonal (in Λ and Σ) spin–orbit interaction are turned on, i.e., calculated from the same values of C_0, C_2, C_4 as before and with a value $A = -602.8\ cm^{-1}$ in the operator AL_zS_z. These can be thought of as the calculated positions of the Hund's case (a) electronic states arising from the $3d^9$ electron configuration in NiF.

The fourth column from the left in Fig. 2 gives the energy levels calculated when the crystal-field interaction and the full spin–orbit interaction are turned on, i.e., calculated from the previous constants and a value of $A = -602.8\ cm^{-1}$ in the operator $A(L_xS_x + L_yS_z)$. These can be thought of as the calculated positions of the Hund's case (c) electronic states arising from the $3d^9$ electron configuration in NiF. They are qualitatively different from the case (a) levels immediately to their left, i.e., the repulsions of levels with the same value of Ω caused by the off-diagonal (in Λ and Σ, but not in Ω) spin–orbit interaction are extremely large on the $2000\ cm^{-1}$ energy scale of this diagram.

The fifth column from the left in Fig. 2 gives the energy levels calculated when the crystal-field interaction and the full spin–orbit interaction are turned on, but when the orbital ladder operator matrix element between $\Lambda = 0$ and $\Lambda = \pm1$ is reduced, as shown in Eq. (13b), by an empirical factor $\beta = 0.878$. These are the levels calcu-

Table 3
Positions of the four observed spin–orbit components arising from the $3d^9$ ground electronic configuration in NiCN, together with residuals, parameter values, and a prediction of the missing $\Omega = 1/2$ state from three least-squares fits of the observed levels. All quantities are in cm^{-1}, except for β, which is unitless.

State[a]	T_0[b]	o–c[c]	o–c[d]	o–c[e]	Const[f]	Value[c]	Value[d]	Value[e]
$\Omega = ½$	_[h]	2796[i]	2730[i]	2672[i]	A	−602.8[g]	−602.8[g]	−602.8[g]
$W_1\,^2\Pi_{3/2}$	2238	9	9	9	β	1.0[g]	0.89[g]	0.78[g]
$X_2\,^2\Delta_{3/2}$	830	−15	−15	−15	C_0	1324(11)	1311(11)	1299(11)
$\Omega = ½$	755	−2	−2	−2	C_2	−589(13)	−570(13)	−554(13)
$X_1\,^2\Delta_{5/2}$	0	8	8	8	C_4	−559(13)	−582(13)	−602(13)

[a] In the notation of Ref. [36]. In the present work, we use only the Ω values to label these states, since Ω is a good quantum number in the non-rotating molecule.
[b] In cm^{-1} from Fig. 16 of Ref. [36] and a suggestion in Ref. [32].
[c] Observed-minus-calculated residuals and parameter values from a fit of the four observed spin–orbit components to the three crystal-field parameters C_0, C_2, and C_4 in Eqs. (10), with $A = -602.8$ cm^{-1} fixed to the Ni^+ free ion value.
[d] Residuals and parameter values from a fit of the four observed spin–orbit components to the three parameters C_0, C_2, and C_4 in Eqs. (10) and (14), with fixed $A = -602.8$ cm^{-1} and $\beta = 0.89$ (as used for NiF in Table 1 and NiCl in Table 2).
[e] Residuals and parameter values from a fit of the four observed spin–orbit components to the three parameters C_0, C_2, and C_4 in Eqs. (10) and (14), with fixed $A = -602.8$ cm^{-1} and $\beta = 0.78$ (arbitrarily chosen).
[f] Parameters from the energy expressions in Eqs. (10) and (14). Numbers in parentheses indicate one standard error (type A, $k = 1$) [45] from the least-squares fit.
[g] Parameter held fixed during the least-squares fit.
[h] This spin–orbit component has not yet been experimentally identified.
[i] Energy for this spin–orbit component predicted from the fit in this column.

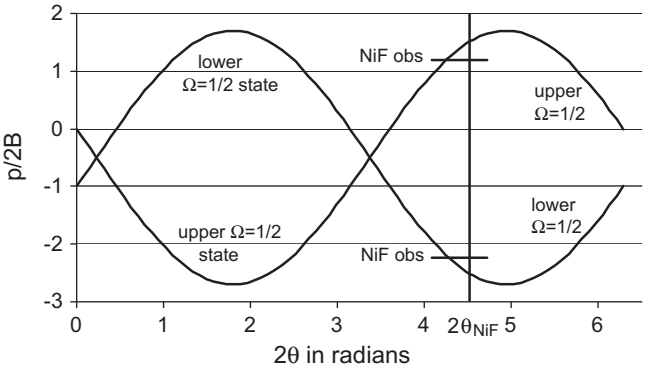

Fig. 3. A plot of $p/2B$ versus $0 \leqslant 2\theta \leqslant 2\pi$, calculated from Eqs. (25), (26), (27a), (27b), (28)–(31) with $\beta = 0.878$ (see Table 1). The theoretical value of 2θ for NiF from these equations is indicated by the vertical line at $2\theta = 4.52$ radians. The intersection of this vertical line with the sinusoidal curves gives the theoretical value of $p/2B$ for the upper and lower $\Omega = 1/2$ states of NiF. The observed values [3] are indicated by short horizontal lines. The discrepancy between theory and experiment can be described in two ways, either by saying that the theoretical value for 2θ is slightly too large, or by saying that the amplitude of the sine curves is slightly too large, but it is probably most useful to say only that this discrepancy indicates the limits of the present somewhat simplified theoretical approach to this problem.

lated in the least-squares fit summarized in columns 5 and 9 of Table 1. Visual comparison of the calculated and observed energy levels in columns 5 and 6 of Fig. 2 shows that their energy differences are almost invisible on a 2000 cm^{-1} scale.

Starting on the right of Fig. 2, we can compare the observed electronic energy levels in NiF with the $^2D_{3/2}$ and $^2D_{5/2}$ energy levels of the free Ni^+ ion. In the author's opinion, the pattern of observed $3d^9$ electronic levels for NiF in column 6 of Fig. 2 makes more sense when viewed as small crystal-field splittings of the Ni^+ atomic ion levels in column 7, than when viewed as large spin–orbit splittings of the case (b) diatomic levels in column 2.

4.2. NiF rotational energy levels in $\Omega = 1/2$ states

We now turn to the question of Ω-type doubling in the two $\Omega = 1/2$ states shown in Fig. 2, which should be proportional to $J^{2\Omega} = J$ [34,37] if interactions with states having other values of Ω can be neglected. Neglect of other states should be a good approximation for low-J transitions in NiF, since electronic state separations are typically hundreds of cm^{-1}, while B values are near 0.4 cm^{-1}, i.e., the relevant Coriolis interaction energy BJ [37] reaches 100 cm^{-1} only for $J \approx 250$.

A pictorial understanding of the p values given by Eqs. (29) and (31) can be obtained from Fig. 3, which gives a plot of $p_{(1)}/2B_{(1)}$ and $p_{(2)}/2B_{(2)}$ (i.e., $p/2B$ for the 1/2 states at lower and higher energy, respectively) against 2θ for the interval $0 \leqslant 2\theta \leqslant 2\pi$, based on curves calculated from the final-fit constants in column 9 of Table 1. These constants and Eq. (25) give a value of $2\theta = 4.52$ rad. The intersection of the vertical line at this value of 2θ in Fig. 3 with the two $p/2B$ curves then predicts values of −2.51 and +1.51 for the lower and upper 1/2 states, respectively.

Molecular constants are reported for these two 1/2 states [3,7], treating them as if they were traditional $^2\Sigma$ states, i.e., treating the splittings within a given N rotational state according to Eq. (23). We can convert the γ values reported in the literature to p values by comparing Eq. (34) with the difference between two levels having the same $J = N + 1/2 = (N + 1) - 1/2$ in Eqs. (23a) and (23b):

$$\begin{aligned}\Delta E_{rot}(^2\Sigma, J = N + 1/2) &= [BN(N+1) + (1/2)\gamma N] - [B(N+1)(N+2) \\ &\quad - (1/2)\gamma(N+2)] \\ &= -2B(N+1) + \gamma(N+1) = (J+1/2)(\gamma - 2B) \\ &= \pm p(J+1/2). \end{aligned} \tag{39}$$

The upper and lower sign choice applies to $^2\Sigma^+$ and $^2\Sigma^-$ electronic states, respectively, as can be seen by noting that $(-1)^{J-1/2} = (-1)^N$ for Eq. (23a), which corresponds to the parity of rotational levels for $^2\Sigma^+$ states, etc. Using the assignments and the B and γ values in Refs. [3,7], we obtain the "experimental" $p/2B$ values (subscript "exp") just to the right of the equal signs below

$$p_{(1)}/2B_{(1)} = -2.23_{\rm exp} \rightarrow -2.23_{\rm exp} \approx -2.51_{\rm theor}, \tag{40a}$$

$$p_{(2)}/2B_{(2)} = -1.19_{\rm exp} \rightarrow +1.19_{chg} \approx +1.51_{\rm theor}. \tag{40b}$$

The theoretical values predicted in this paper (subscript "theor") are given following the ≈ signs. The value following the arrow in Eq. (40b) (subscript "chg") is the experimental value with its sign changed to bring it into agreement with the theoretically predicted sign (see below).

The values following the arrows in Eq. (40) are in reasonable agreement with the theoretical values. It is interesting to note that the sum of these two $p/2B$ values is −1.04, which is within 4% of the theoretical value of −1 given in Eq. (37a), even though the two $p/2B$ values themselves are only 89% and 79% of their predicted values.

As a possible contribution to the 4% difference from unity of the sum of the two $p/2B$ values, we recall that the present model assumes a single B value for all states arising from the $3d^9$ configuration, whereas the B values reported for the two 1/2 states under discussion here differ from each other by 1%. This fact requires further investigation, however, since the reported B values may just be effective rotational constants, i.e., constants containing contributions from L and/or S uncoupling effects, much as the B values for the two spin components of a case (a) $^2\Pi$ state do [34].

The values following the arrows are shown graphically as short horizontal lines crossing the vertical line at 4.52 rad in Fig. 3. If agreement between theory and experiment were perfect, intersections of the short horizontal lines and the vertical line would fall exactly on the $p/2B$ versus 2θ curves.

We turn now to a more detailed discussion of the experimental determination of the relative and absolute parity [34] of rotational levels in the nickel halides. The relative parity can in principle be determined experimentally, since observed dipole-allowed transitions can be used to divide rotational states into one group with one parity and another group with the other parity. Relative parities can be used to obtain a consistency check on the relative signs of the p constants, which is actually of some importance because of the theoretical prediction that the two correctly signed p constants must sum to $-2B$. As indicated above and in Fig. 3, the p values for the two $\Omega = 1/2$ states in NiF should have opposite signs, which leads to the conclusion that for given J value, the upper (lower) rotational energy level of the upper $\Omega = 1/2$ spin–orbit state has the same parity as the lower (upper) rotational level of the lower $\Omega = 1/2$ state. To assign relative parities in NiF, we look (in the simplest case) for a pair of electronic transitions which connect the two $\Omega = 1/2$ states from the $3d^9$ manifold to the same upper state, which itself should have a measurable Ω-type doubling. Fig. 1 of Ref. [3] indicates that four candidate pairs of such transitions have already been observed, one pair from the [19.7] $\Omega = 3/2$ upper state, one pair from [20.1] $\Omega = 1/2$, one pair from [23.0] $\Omega = 3/2$, and one pair from [23.5] $\Omega = 1/2$. However, for the first, second, and third of these pairs only one of the two transitions has been rotationally analyzed. For the fourth pair neither transition has been rotational analyzed. Examination of all the NiF data [1–7] indicates that a more indirect way of connecting the two $\Omega = 1/2$ states is also not available. Thus, until additional rotational analyses are published, relative parities of the rotational levels of the two $\Omega = 1/2$ states from the $3d^9$ manifold cannot be assigned experimentally. For this reason, it is does not contradict the presently available experimental information to change the sign of $p_{(2)}$ without changing the sign of $p_{(1)}$ in Eq. (40), since the former can be accomplished simply by exchanging the e and f labels on all branches in the observed line list for the [22.9] $^2\Pi_{3/2} - [1.5]$ $B^2\Sigma^+$ transition in Table 1 of Ref. [3].

Absolute parities can only be assigned on the basis of some theoretical model. In the present paper, we have essentially done that in Section 2. With the conventions adopted, absolute parities of the rotational levels of the two $\Omega = 1/2$ states in the $3d^9$ manifold are determined by Eq. (34a) and (34b) and the calculated sign of p in Eq. (29) and (31). For example, for $p > 0$ and even values of $J - 1/2$, the positive parity state of given J lies above the negative parity state for that J. Absolute parities assigned in this way can then be used to label $+ \leftrightarrow -$ transitions as electric-dipole allowed, to label $+ \leftrightarrow +$ and $- \leftrightarrow -$ transitions as magnetic-dipole or electric-quadrupole allowed, to restrict consideration of perturbations to pairs of levels with the same parity, etc.

4.3. NiCl electronic energy levels

We now repeat the procedures in Sections 4.1 and 4.2 for NiCl. Columns 1 and 2 of Table 2 give labels and positions in cm^{-1} of the five $3d^9$ spin–orbit components of NiCl taken from Fig. 1 of Ref. [10]. Column 3 gives observed-minus-calculated residuals from a least-squares fit of these levels to the four parameters A, C_0, C_2, and C_4, using the expressions in Eq. (10). These residuals are again large (as for NiF) and evenly distributed among the five levels. Column 7 gives the parameter values obtained from this fit. The magnitude obtained for the spin–orbit constant A is again poorly determined and somewhat smaller than that in the free Ni^+ ion.

Column 4 gives residuals from a fit of the five levels to the three crystal-field parameters C_0, C_2, and C_4, with the spin–orbit constant fixed to its value in Ni^+, as shown by the constants from this fit given in column 8. These residuals resemble those for NiF and again suggest that something may be wrong with the treatment of the $\Omega = 1/2$ states. Column 4 in Fig. 4 shows the energy levels calculated from this fit. Comparison of these calculated levels with the observed levels shown in column 6 of Fig. 4 shows that the $\Omega = 1/2$ states have again been "pushed apart" too far by the model, and their observed separation of 1386 cm^{-1} in NiCl is again smaller than the minimum of 1476 cm^{-1} required by the off-diagonal matrix element $+(3/2)^{1/2}A = -738$ cm^{-1} when the Ni^+ value for A is used.

Column 5 of Table 2 shows that the empirical correction factor β is again quite effective in reducing the residuals, since they are all 8 cm^{-1} or less with A fixed to -602.8 cm^{-1} and β optimized to 0.897. Constants from this fit are given in column 9. We note that the exact fit of five lines to five parameters (not shown) gives the values $A = -608.2187$ cm^{-1} and $\beta = 0.89144$.

The long discussion of Fig. 2 given earlier for NiF could be repeated here almost without change for Fig. 4 of NiCl. Instead we simply note that the observed levels for NiCl cluster even more closely around the $^2D_{3/2}$ and $^2D_{5/2}$ atomic ion states.

4.4. NiCl rotational levels in $\Omega = 1/2$ states

Fig. 5 gives a plot of $p_{(1)}/2B_{(1)}$ and $p_{(2)}/2B_{(2)}$ (i.e., $p/2B$ for the 1/2 states at lower and higher energy, respectively) against 2θ for the

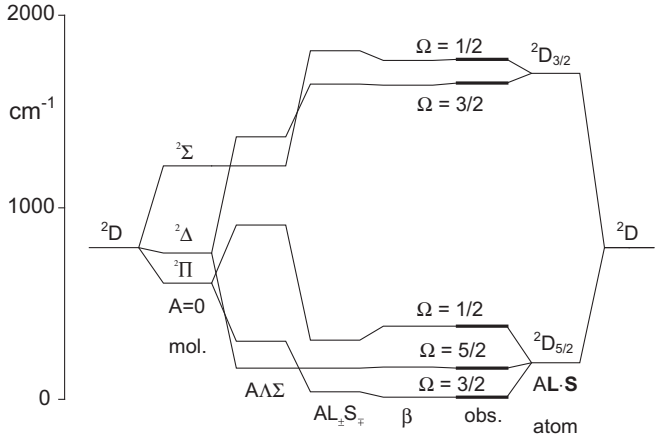

Fig. 4. Energy levels of NiCl calculated when various interactions in Eqs. (10) and (14) are "turned on" sequentially, as in Fig. 2. Column 1 gives the ^2D state of Ni^+. Column 2 gives the case (b) $^2\Sigma$, $^2\Pi$, $^2\Delta$ states of NiCl calculated from C_0, C_2, C_4 in column 8 of Table 2 and $A = 0$. Column 3 gives the case (a) $^2\Sigma$, $^2\Pi_{1/2}$, $^2\Pi_{3/2}$, $^2\Delta_{3/2}$, and $^2\Delta_{5/2}$ states calculated from C_0, C_2, C_4 in column 8 of Table 2 and $-602.8(L_zS_z)$. Column 4 gives the case (c) levels calculated from C_0, C_2, C_4 in column 8 of Table 2 and $-602.8(\boldsymbol{L}\cdot\boldsymbol{S})$. Column 5 gives the energy levels calculated in the least-squares fit of columns 5 and 9 in Table 2, where both the crystal-field interaction and the full spin–orbit interaction are turned on, and where the matrix element between $\Lambda = 0$ and $\Lambda = \pm 1$ is reduced by an empirical factor $\beta = 0.897$. The thick lines in column 6 give the observed levels [10], which are probably better viewed as arising from small crystal-field splittings of the Ni^+ atomic ion levels in column 7, than as arising from large spin–orbit splittings of the case (b) levels in column 2.

interval $0 \leqslant 2\theta \leqslant 2\pi$, based on curves calculated from the final-fit constants in column 9 of Table 2. These constants and Eq. (25) give a value of $2\theta = 4.42$ rad. The intersection of the vertical line at this value of 2θ in Fig. 5 with the two $p/2B$ curves then predicts values of −2.46 and +1.46 for the lower and upper 1/2 states, respectively.

For NiCl, rotational analyses involving both of the $3d^9$ $\Omega = 1/2$ states have been reported [9,11,13]. Converting the γ value in Table 3 of Ref. [9] to a $p_{(2)}$ value as described in connection with Eq. (40), and taking the $p_{(1)}$ value directly from Table 1 of Ref. [13], we obtain the experimental values for $p/2B$ following the equal signs below.

$$p_{(1)}/2B_{(1)} = +2.32_{\text{exp}} \rightarrow -2.32_{\text{chg}} \approx -2.46_{\text{theor}}, \tag{41a}$$

$$p_{(2)}/2B_{(2)} = -1.32_{\text{exp}} \rightarrow +1.32_{\text{chg}} \approx +1.46_{\text{theor}}. \tag{41b}$$

The theoretical numbers obtained here for these same quantities are given following the ≈ signs. The numbers following the arrows (with subscript "chg") are again the experimental values, but with their signs changed to agree with the theoretical predictions (see below). These changed values differ by only 6% and 11%, respectively, from the theoretical predictions. They are also shown graphically as short horizontal lines in Fig. 5.

For NiCl it is quite useful to look more closely at the relative signs of the p values, since these can be determined experimentally from line lists for the [12.3] $^2\Sigma^+ - B^2\Sigma^+$ transition [11] and for the [12.3] $^2\Sigma^+ - X^2\Pi_{1/2}$ transition [13], which share a common upper state having measureable Ω-type doubling. It can easily be shown that

$$[R_{ff}(J) - P_{ee}(J)]_{(12.3-X)} - [R_{ff}(J) - P_{ee}(J)]_{(12.3-B)} \approx (J + 1/2)[p_{(1)} - p_{(2)}], \tag{42}$$

where the ≈ sign indicates that centrifugal distortion and other higher order corrections are not taken into account. Carrying out this calculation for $J = 46.5$, 47.5, and 48.5 in the line lists of Refs. [11,13], and dividing by $(J + 1/2)$ and twice the average B value, we obtain

$$[p_{(1)} - p_{(2)}]/[B_{(1)} + B_{(2)}] = 3.61, 3.61, \text{ and } 3.60. \tag{43}$$

The experimentally determined magnitudes (for three different J values) of the expression in Eq. (43) are consistent with the experimentally determined values for $p/2B$ in Eq. (41) only if $p_{(1)}/2B_{(1)}$ and $p_{(2)}/2B_{(2)}$ have opposite signs, as predicted by theory and as reflected in the different experimental signs just after the equality in Eq. (41a) and (41b).

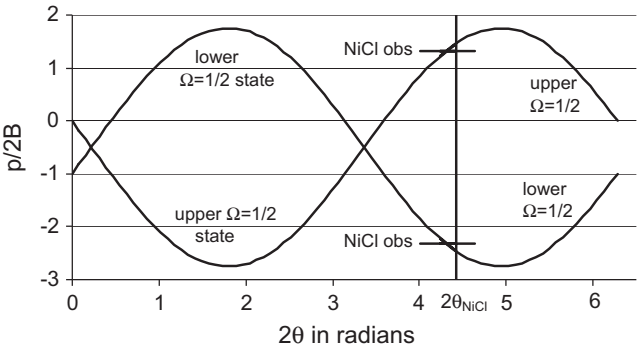

Fig. 5. A plot of $p/2B$ versus $0 \leqslant 2\theta \leqslant 2\pi$, as calculated from Eqs. (25), (26), (27a), (27b), (28)–(31) with $\beta = 0.897$ (see Table 2). The theoretical value of 2θ for NiCl from these equations is indicated by the vertical line at $2\theta = 4.42$ radians. The intersection of this vertical line with the sinusoidal curves gives the theoretical value of $p/2B$ for the upper and lower $\Omega = 1/2$ states of NiCl. The observed values [9,11,13] are indicated by short horizontal lines. The discrepancy between theory and experiment, which is somewhat smaller than that for NiF in Fig. 3, can again be described by saying that the theoretical value of 2θ for NiCl is slightly too large, or that the amplitude of the sinusoidal curves is slightly too large.

As mentioned earlier, absolute parities cannot be determined experimentally, and the signs of all three values in Eq. (43) would be reversed if the subscript exchange $e \leftrightarrow f$ were carried out on all branch labels for the [12.3] $^2\Sigma^+ - B^2\Sigma^+$ transition in Table 2 of Ref. [11] and for the [12.3] $^2\Sigma^+ - X^2\Pi_{1/2}$ transition in Table 2 of Ref. [13] (as well as on branch labels for transitions involving [1.7] $^2\Sigma^+$ in Ref. [9]). This exchange would then give the signed $p/2B$ values following the arrows in Eq. (41), which agree with those predicted by theory. The author obviously favors making such an $e \leftrightarrow f$ exchange, so it is now of interest to examine what changes this would require in the original symmetry species and quantum number assignments and in the original molecular fitting parameters. There are three cases.

An $e \leftrightarrow f$ exchange is quite simple for $\Omega = 1/2$ states that have been treated as $^2\Pi_{1/2}$ states: All J assignments are kept unchanged. The parities of all levels are changed $+ \leftrightarrow -$. The signs of all Ω-doubling parameters (i.e., of p and its centrifugal distortion corrections) are changed. All other molecular constants are kept unchanged. This is exactly the situation for the $X^2\Pi_{1/2}$ state used to determine $p_{(1)}$ above. (Note that an analogous procedure would also apply to states that have been treated as $^2\Pi_{3/2}$, $^2\Delta_{3/2}$, $^2\Delta_{5/2}$, etc.)

The next simplest situation corresponds to one possibility for carrying out an $e \leftrightarrow f$ exchange for $\Omega = 1/2$ states that have been treated as $^2\Sigma^+$ states, i.e., treated using the spin-splitting parameter γ: All N and J assignments and all molecular constants are kept unchanged. The parities of all levels are changed $+ \leftrightarrow -$. The $^2\Sigma^+$ electronic symmetry species is changed to $^2\Sigma^-$. At first this seems like a rather drastic thing to do, but Zou and Liu have already suggested [31], based on their ab initio calculations, that the [12.3] $^2\Sigma^+$ assignment in Refs. [11,13] should be changed to [12.3] $^2\Sigma^-$. This is exactly what is required for the $e \leftrightarrow f$ exchange proposed here. (Note that an analogous procedure could also be applied to states that were originally treated as $^2\Sigma^-$.)

The most complicated situation corresponds to the other possibility for carrying out an $e \leftrightarrow f$ exchange for states treated as a $^2\Sigma^+$ state, i.e., treated using the spin-splitting parameter γ: The J assignments, the $^2\Sigma^+$ assignment, and all molecular constants except γ (and its centrifugal distortion correction terms) and the band origin ν_0 are kept unchanged. The parities of all levels are changed $+ \leftrightarrow -$. $N = J \pm 1/2$ assignments are all changed to $N = J \mp 1/2$. The γ value is changed to $4B - \gamma$. The band origin is changed to $\nu_0 + 2B - \gamma$. This is exactly the situation for the $B^2\Sigma^+$ state used to determine $p_{(2)}$ above. (Note that an analogous procedure could also be applied to states that were originally treated as $^2\Sigma^-$.)

4.5. NiBr, NiI, and NiCN

The positions of only two of the five spin–orbit components from the $3d^9$ configuration have been published for NiBr [15,16] and NiI [18–20]. None of the four known states for NiBr and NiI have $\Omega = 1/2$.

Four spin–orbit components of the $3d^9$ manifold, with $\Omega = 5/2$, 3/2, 3/2, and 1/2 have been observed for the related molecule NiCN [32,36]. The present model should in principle be applicable to unperturbed vibrationless electronic states in this molecule, which provides an opportunity to predict the missing $\Omega = 1/2$ level. Table 3 shows three fits of the four observed positions to the crystal-field parameters C_0, C_2, and C_4 of the present formalism, with A fixed to the Ni^+ free ion value of −602.8 cm^{-1}, and with $\beta = 1.00$ (no empirical correction to the matrix element $\langle \Lambda = +1|L_+|\Lambda = 0\rangle$ in Eq. (13b)), $\beta = 0.89$ (similar to the values used for NiF in Table 1 and NiCl in Table 2), and $\beta = 0.78$ (arbitrarily chosen). In contrast to the fits for NiF and NiCl, these values for β all lead to the same

(and to rather large) residuals in the NiCN fit. It is thus possible that the present formalism is less suitable for triatomics than for diatomics, presumably because the presence of four vibrational degrees of freedom in a linear triatomic molecule, instead of only one, as in the diatomic nickel monohalides, gives rise to many more opportunities for randomly distributed vibronic perturbations.

In spite of this concern, Table 3 gives the predicted position of the missing $\Omega = 1/2$ state obtained from each of the three fits. The author prefers the prediction at 2730 cm^{-1}, obtained from the fit with $\beta = 0.89$, since similar β values were needed for NiF and NiCl, but in fact none of the predicted positions in Table 3 are far from the 2773 cm^{-1} position predicted by ab initio calculations [32].

4.6. NiH

As mentioned earlier, the large rotational constants of 7 or 8 cm^{-1} for electronic states of NiH [22,26] make the truncated 2×2 matrix approximation used in the present treatment of rotational energy levels invalid. The treatment of the five spin–orbit components of the $3d^9$ manifold in the non-rotating NiH molecule could in principle still be carried out, but for such a treatment to be accurate at the 1 cm^{-1} level, all reported band origins would have to be carefully corrected for various contributions arising from $B[\boldsymbol{J}^2 - J_z^2 + \boldsymbol{L}^2 - L_z^2 + \boldsymbol{S}^2 - S_z^2]$ in the rotational Hamiltonian of Eq. (15). This brings up the problem of what empirical correction to apply to the nominal value of $\langle \boldsymbol{L}^2 \rangle = 6$, or $B\langle \boldsymbol{L}^2 \rangle \approx 45$ cm^{-1}. For these various reasons, we will not consider NiH in this paper.

5. Discussion

A simple additional test of the formalism in this paper would be to rotationally analyze one of the several pairs of transitions in NiF connecting a given upper state to both $\Omega = 1/2$ states in the $3d^9$ manifold [10], since this would experimentally confirm or disprove the proposed change of only one sign in Eq. (40), i.e., confirm or disprove the theoretical prediction that $p_{(1)}$ and $p_{(2)}$ have opposite signs in NiF. If the relative signs of the p values from such analyses agree with the present theory, it would then be the author's opinion that the e, f labels (and therefore the parity labels) should be revisited for all observed transitions in NiF and NiCl, to bring both the signs of the p values of the $\Omega = 1/2$ states as well as the ± character of the [12.3] $^2\Sigma$ state into agreement with theory, and then to make the e, f assignments in all other presently observed transitions consistent with these changes.

Other tests of the present formalism involve the more difficult task of finding and rotationally analyzing the remaining $3d^9$ spin–orbit components in NiBr and NiI, or of studying the $4d^9$ spin–orbit components in the palladium halides. As mentioned above, triatomics like NiCN may be less favorable molecules for formalism-testing purposes, since the four vibrational degrees of freedom greatly increase the chances of accidental vibronic resonances causing unwanted perturbations in the positions of the excited electronic states of the $3d^9$ manifold.

If sufficient confidence in the present formalism can be established, then it might be desirable to extend it to a determination of the experimentally observed Ω-doubling parameters in various $\Omega = 3/2$ states. Such an extension would probably only involve applying second-order perturbation theory to the rotationally induced mixing of each $\Omega = 3/2$ state with both $\Omega = 1/2$ states in the d^9 manifold, i.e., to the L and S uncoupling induced by $J_{\pm}L_{\mp}$ and $J_{\pm}S_{\mp}$. This second-order perturbation theory would also lead to "corrected" B values for the $\Omega = 1/2$ states (i.e., to B values more closely related to the internuclear distance).

Finally we consider, with the help of Fig. 1a and b, the somewhat confusing question of exactly which Hund's coupling case [34] best describes the five spin–orbit components of the three orbital electronic states occurring in the $3d^9$ manifold. At the extreme left of these figures, i.e., at −1 on the abscissa, we clearly have three Hund's case (b) states. At the extreme right (at +1 on the abscissa) it seems reasonable to say that we have Hund's case (e) states, since $\boldsymbol{L}$ and $\boldsymbol{S}$ are coupled to form a resultant electronic angular momentum $\boldsymbol{J}_e = \boldsymbol{L} + \boldsymbol{S}$, and the projection Ω_e of $\boldsymbol{J}_e$ is not coupled to the internuclear axis (i.e., there is no energy difference between the different Ω_e states for a given J_e). For the rest of the discussion, we assume that we are considering rotational levels for which $BJ/|(A + C_2)| \ll 1$ in Fig. 1a or $BJ/|(A - C_2)| \ll 1$ in Fig. 1b. (As mentioned earlier, these inequalities will normally be satisfied for the usually observed rotational levels in the nickel halides, but will normally not be satisfied for the usually observed rotational levels of nickel hydride.) Moving a little to the right of −1 on the abscissa, the Δ state in Fig. 1a, and the Δ and Π states in Fig. 1b, will behave like case (a) states, since spin–orbit splittings are large compared to BJ. The Π state in Fig. 1a would probably behave more like case (b), since its spin–orbit splitting is quite small at values between −1.0 and −0.5 on the abscissa.

The most difficult question arises when we move somewhat to the left of +1 on the abscissa, since then: (i) $\boldsymbol{L}$ and $\boldsymbol{S}$ are still coupled to form a resultant $\boldsymbol{J}_e = \boldsymbol{L} + \boldsymbol{S}$, and (ii) the projection Ω_e of $\boldsymbol{J}_e$ is coupled to the internuclear axis by energies larger than BJ, but (iii) the usual projections Λ (of $\boldsymbol{L}$) and Σ (of $\boldsymbol{S}$) along the internuclear axis are not good quantum numbers. As we have seen above, a position a little to the left of +1 on the abscissa corresponds to the actual situation in NiF and NiCl (and probably also to the situation in NiBr and NiI, though there is no experimental proof of this yet.) Following Ref. [34], it is possible to rule out for states lying between +0.7 and +0.8 on the abscissa: case (a), because Λ and Σ are not defined (are not good quantum numbers), as well as cases (b), (d), and (e), because Ω_e is well defined. In an early discussion of Hund's coupling cases [46], Mulliken defined a case (c), which corresponds exactly to this situation, namely $\boldsymbol{L}$ and $\boldsymbol{S}$ are coupled to form a resultant $\boldsymbol{J}_e = \boldsymbol{L} + \boldsymbol{S}$, the projection $\Omega_e \equiv \Lambda + \Sigma$ of $\boldsymbol{J}_e$ is coupled to the internuclear axis (i.e., $\Omega \equiv \Omega_e$ is a good quantum number), but Λ and Σ are not individually good quantum numbers. Mulliken noted in that 1930 paper [46], that no examples of this case (c) had yet been found. In 1931 Mulliken expanded his definition of case (c) [47] to its modern form [34], i.e., to states in which only Ω_e is a good quantum number, and then applied that label to a number of molecules. The author is certainly in favor of keeping the well-established modern definition of case (c), i.e., to require for case (c) that only Ω_e be a good quantum number in the non-rotating molecule, but then to add a prime, i.e., to use the label case (c′), when J_e is also a good quantum number, as it was in Mulliken's original definition of case (c). Figs. 2 and 4 then indicate that NiF is close, and NiCl is closer, to this Hund's case (c′) limit.

States near the middle of Fig. 1a or b are not near any limiting Hund's coupling case, and are therefore probably most conveniently referred to as "intermediate coupling" states.

Acknowledgments

The author is greatly indebted to T. Okabayashi, A.J. Merer, and especially L.C. O'Brien for extremely helpful comments and criticism of an early draft of this paper.

References

[1] A. Bouddou, C. Dufour, B. Pinchemel, J. Mol. Spectrosc. 168 (1994) 477–482.
[2] C. Dufour, B. Pinchemel, J. Mol. Spectrosc. 173 (1995) 70–78.

[3] Y. Krouti, T. Hirao, C. Dufour, A. Boulezhar, B. Pinchemel, P.F. Bernath, J. Mol. Spectrosc. 214 (2002) 152–174.
[4] B. Pinchemel, T. Hirao, P.F. Bernath, J. Mol. Spectrosc. 215 (2002) 262–268.
[5] J. Jin, Y. Chen, X.-L. Yang, Q. Ran, C.-X. Chen, J. Mol. Spectrosc. 208 (2001) 18–24.
[6] J. Jin, Q. Ran, X.-L. Yang, Y. Chen, C.-X. Chen, J. Phys. Chem. A. 105 (2001) 11177–11182.
[7] M. Tanimoto, T. Sakamaki, T. Okabayashi, J. Mol. Spectrosc. 207 (2001) 66–69.
[8] T. Hirao, C. Dufour, B. Pinchemel, P.F. Bernath, J. Mol. Spectrosc. 202 (2000) 53–58.
[9] A. Poclet, Y. Krouti, T. Hirao, B. Pinchemel, P.F. Bernath, J. Mol. Spectrosc. 204 (2000) 125–132.
[10] Y. Krouti, A. Poclet, T. Hirao, B. Pinchemel, P.F. Bernath, J. Mol. Spectrosc. 210 (2001) 41–50.
[11] C.A. Rice, L.C. O'Brien, J. Mol. Spectrosc. 221 (2003) 131–134.
[12] S. Tumturk, L.C. O'Brien, J.J. O'Brien, J. Mol. Spectrosc. 225 (2004) 225–229.
[13] C.A. Rice, T.L. Kellerman, B. Owen, L.C. O'Brien, H. Cao, J.J. O'Brien, J. Mol. Spectrosc. 235 (2006) 271–274.
[14] E. Yamazaki, T. Okabayashi, M. Tanimoto, Astrophys. J. Lett. 551 (2001) L199–L201.
[15] J.W.-H. Leung, X.-H. Wang, A.S.-C. Cheung, J. Chem. Phys. 117 (2002) 3694–3700.
[16] J.-J. Ye, J.W.-H. Leung, A.S.-C. Cheung, J. Chem. Phys. 125 (2006) 214308-1–214308-8.
[17] E. Yamazaki, T. Okabayashi, M. Tanimoto, J. Chem. Phys. 121 (2004) 162–168.
[18] W.S. Tam, J.W.-H. Leung, S.-M. Hu, A.S.-C. Cheung, J. Chem. Phys. 119 (2003) 12245–12250.
[19] W.S. Tam, J.-J. Ye, A.S.-C. Cheung, J. Chem. Phys. 121 (2004) 9430–9435.
[20] T.-M. Ma, L. Li, J.W.-H. Leung, A.S.-C. Cheung, Chin. J. Chem. Phys. 22 (2009) 611–614.
[21] T. Miyazawa, E.Y. Okabayashi, F. Koto, M. Tanimoto, T. Okabayashi, J. Chem. Phys. 124 (2006) 224321-1–224321-5.
[22] R. Scullman, S. Löfgren, S.A. Kadavathu, Phys. Scr. 25 (1982) 295–301.
[23] J.A. Gray, S.F. Rice, R.W. Field, J. Chem. Phys. 82 (1985) 4717–4718.
[24] J.A. Gray, R.W. Field, J. Chem. Phys. 84 (1986) 1041–1042.
[25] J.A. Gray, M.-G. Li, R.W. Field, J. Chem. Phys. 92 (1990) 4651–4659.
[26] S.A. Kadavathu, R. Scullman, J.A. Gray, M.-G. Li, R.W. Field, J. Mol. Spectrosc. 140 (1990) 126–140.
[27] J.A. Gray, M.-G. Li, T. Nelis, R.W. Field, J. Chem. Phys. 95 (1991) 7164–7178.
[28] E.M. Spain, M.D. Morse, J. Chem. Phys. 97 (1992) 4641–4660.
[29] P. Carette, C. Dufour, B. Pinchemel, J. Mol. Spectrosc. 161 (1993) 323–335.
[30] C.-L. Yang, F. Gao, X.-Y. Zhang, K.-L. Han, J. Chem. Phys. 123 (2005). 204308-1–204308-6.
[31] W.-L. Zou, W.-J. Liu, J. Chem. Phys. 124 (2006) 154312-1–154312-16.
[32] T. Hirano, R. Okuda, U. Nagashima, K. Tanaka, P. Jensen, Chem. Phys. 346 (2008) 13–22.
[33] Yu. Ralchenko, A.E. Kramida, J. Reader, NIST ASD Team, 2008. NIST Atomic Spectra Database (Version 3.1.5) <http://physics.nist.gov/asd3>.
[34] G. Herzberg, The Spectra of Diatomic Molecules, Van Nostrand, Princeton, 1950.
[35] W. Moffitt, C.J. Ballhausen, Ann. Rev. Phys. Chem. 7 (1956) 107–136.
[36] C.T. Kingston, A.J. Merer, T.D. Varberg, J. Mol. Spectrosc. 215 (2002) 106–127.
[37] J.T. Hougen, The Calculation of Rotational Energy Levels and Rotational Line Intensities in Diatomic Molecules, NBS Monograph 115, 1970. <http://www.nist.gov/physlab/data/molspecdata.cfm>.
[38] E.U. Condon, G.H. Shortley, The Theory of Atomic Spectra, Cambridge, 1964.
[39] B. Bleaney, K.W.H. Stevens, Rep. Prog. Phys. 16 (1953) 108–159.
[40] J.T. Hougen, J. Chem. Phys. 36 (1962) 519–534.
[41] I. Kopp, J.T. Hougen, Can. J. Phys. 45 (1967) 2581–2596.
[42] J.T. Hougen, J. Mol. Spectrosc. 42 (1972) 381–384.
[43] N.J. Bridge, J. Mol. Spectrosc. 42 (1972) 370–380.
[44] J.M. Brown, J.T. Hougen, K.-P. Huber, J.W.C. Johns, I. Kopp, H. Lefebvre-Brion, A.J. Merer, D.A. Ramsay, J. Rostas, R.N. Zare, J. Mol. Spectrosc. 55 (1975) 500–503.
[45] B.N. Taylor, C.E. Kuyatt, NIST Technical Note No. 1297 (1994), Guidelines for Evaluating and Expressing the Uncertainty of NIST Measurement Results, <http://physics.nist.gov/Pubs/guidelines/contents.html>.
[46] R.S. Mulliken, Rev. Mod. Phys. 2 (1930) 60–115.
[47] R.S. Mulliken, Rev. Mod. Phys. 3 (1931) 89–155.